ATLAS FORWARD PHYSICS

REPORT TO ATLAS REVIEW COMMITTEE

5 July 2009

1. Introduction

This report addresses issues raised by the ATLAS AFP Review Committee in February and in its report of 18th May. Significant work has been performed over the last few months. An executive summary of the progress is provided here, with extended reports attached in the Appendix. The proposed schedule is discussed in a separate note.

Comments from the committee are given in ***"quotes"***.

2. Physics case

"Physics: the Review Panel encourages the proponents to strengthen the physics case of the proposed detector, especially the possibility to confirm the quantum numbers of a potential Higgs signal This should include realistic assumptions on trigger bandwidth (see trigger section below), as well as realistic background estimations"

2.1 Overview of the physics case

The physics case for the addition of precision proton detectors in the high dispersion regions 220 m and 420 m either side of the ATLAS detector has been discussed in detail in the AFP Letter of Intent to ATLAS, which is largely based on the FP420 R&D report [1]. The initial FP420 R&D programme was endorsed by the LHCC in 2005: "The LHCC acknowledges the scientific merit of the FP420 physics program and the interest in its exploring its feasibility." The addition of proton detectors in the 220 m region as well as at 420 m further strengthens the physics case by increasing the acceptance over a wide mass range of potential resonances. The addition of AFP to ATLAS enables the LHC to operate as a gluon-gluon or photon-photon collider with known centre-of-mass energy in the range of 70 GeV to 1.4 TeV. The mass acceptance for 420-420, 220-420 and 220-220 is shown in Fig. 4.3. AFP provides a rich QCD and electroweak physics programme extending the current ATLAS physics capabilities. Photon-photon physics complements the ATLAS strategy for precision limits (or measurements) of anomalous couplings and the search for supersymmetric (and other BSM) charged particles. Furthermore, gluon-gluon physics allows the study of Higgs bosons in the central exclusive production (CEP) channel. In addition to a mass measurement of about 3 GeV on an event-by-event basis, the observation of a Higgs boson in this channel is equivalent to a quantum number measurement because resonance production is heavily suppressed for particles that do not have $J^{PC}=0^{++}$.

The capability of precision forward proton detectors to measure Higgs boson properties has been extensively studied in the literature over the last four years [2]:

- The Standard Model $H \to WW^*$ channel has been studied, with the conclusion that the semi-leptonic and fully leptonic decay channels can be measured for 140 GeV < M_H < 200 GeV. For the small α_{eff} scenario in the MSSM, it is perhaps possible to study the Higgs boson down to 120 GeV.
- The $h, H \to b\bar{b}, \tau\tau$ channels have been studied for the MSSM, tri-mixing, triplet, and 4th generation Higgs sectors, with the conclusion that AFP could observe these channels for a large area of parameter space in each model. There are also other models (NMSSM, CPX) in which the bb/ττ channels could be studied using AFP.
- The $h \to aa \to 4\tau$ decay channel has been studied, and demonstrated viable, for the NMSSM. It should be noted that similar topologies occur in other models such as CPX.

The full physics potential of AFP has yet to be completely explored. The increased interest recently from both experimentalists and theorists is likely to uncover more models/channels in which AFP could be beneficial to the ATLAS Higgs community. For example at the recent EDS conference at CERN, one presentation showed that if a 4th fermion generation is combined with a Standard Model Higgs, then with CEP it possible to measure $H \to b\bar{b}$ at low luminosity and $H \to \tau\tau$ at high luminosity [3].

Our goal in this section is to strengthen the AFP Higgs physics case, by validating the conclusions made in these papers. In particular, there were several critical assumptions that needed to be evaluated:

1) A viable L1 trigger strategy needed to be demonstrated for the $h, H \to b\bar{b}$ channel, as some papers ignored trigger issues, and others assumed a large available Level 1 bandwidth. In particular, the review committee asked AFP to demonstrate a high signal efficiency given a L1 bandwidth of about 2 kHz. Significant progress in developing a L1 trigger is described in Sec. 2.2.

2) The phenomenological papers tend to use optimistic assumptions for the position of the detectors with respect to the beam, which determines the acceptance. Figure 4.3 shows the most recent calculation of the acceptances taking into account our latest understanding of the beam optics and detector constraints. These acceptances have been used in the latest physics studies.

3) The exclusivity cuts presented in the literature were studied at generator level with detector resolution/efficiencies taken from the ATLAS TDR (1999). These criteria needed to be validated using standard ATLAS detector simulation, especially for a central tracking variable that eliminated a large fraction of pile-up background. Work in this area is discussed in Section 2.4.

Finally, realistic running scenarios for AFP are required. This point is discussed in Section 2.5. The significant progress that has been made in all these areas is summarised in the following sections.

2.2 Level 1 Triggering

"Clarify which physics processes need dedicated trigger bandwidth and which physics processes can be studied without requiring a special trigger. The trigger bandwidth requested is high at Level 1 (30 kHz was shown + 15 kHz for alignment)".

2.2.1 Level 1 triggering for $H \to b\bar{b}$

The $H \to b\bar{b}$ decay is the only channel that requires significant dedicated bandwidth at Level 1. A substantial effort was undertaken to improve this L1 trigger to reduce the bandwidth to acceptable levels. The resulting ATLAS note, ATL-COM-DAQ-2009-062 (see also Appendix), shows that this can be attained with a combination of a trigger signal from a tagged proton at 220 m with calorimeter information.

The table below summarises the progress that has been made in this area. Using calorimeter information it is possible to reduce the total rate of the $H \to b\bar{b}$ trigger by a factor of 20 to 2.9 kHz at L= 10^{34} $cm^{-2}s^{-1}$. Progress since the review is shown in the table by shading the relevant cells. The last two rows of the table represent different options and are not sequential cuts.

Trigger Condition	L= 2 x 10^{33} $cm^{-2}s^{-1}$ (kHz)	L= 10^{34} $cm^{-2}s^{-1}$ (kHz)
J23 + J35	52	261
J23 + J35+ P220	3.7	90
J23 + J35 + P220 + pseudorapidity	0.7	17
J23 + J35 + P220 + pseudorapidity + Δφ	0.61	14.8
J23 + J35 + P220 + pseudorapidity + f_T	0.12	2.9

Key conclusions from the trigger note:

The $H \to b\bar{b}$ channel is one of the most challenging for the proposed AFP upgrade, due to the low signal cross section and large background. Successful measurements will depend on the implementation of an efficient trigger with low pre-scale. A di-jet trigger based only on central detectors is not sufficient to keep a reasonably low L1 rate without large prescales, so information from the AFP detector stations will be required in addition to an upgrade of the L1 calorimeter trigger. Specifically:

• To have high efficiency and reasonable rejection for a light Higgs, the forward proton trigger must have the capability to trigger on the subset of protons that hit the inner 4 mm of the detector station at 220 m.

• The L1 calorimeter must provide the E_T, η and φ of each jet ROI (region of interest) so that the exclusivity conditions can be implemented. Although this information is calculated at L1, it is not currently available for trigger rejection. Discussions with trigger experts indicate that the L1 calorimeter Phase I upgrade is expected to address this issue on the 2013 time scale, allowing this information to be used at L1.

This combination makes it possible to reduce the rates for jet E_T thresholds that provide a reasonable efficiency for low-mass Higgs detection. This should be true even up to the highest luminosities for the exclusivity conditions based on angular information. An additional factor of five rejection was observed for the exclusivity criterion, f_T , which utilizes the ratio between jet transverse energies and the total scalar sum of transverse energy in the detector. However, further work with (currently unavailable) pile-up samples is necessary to determine the effect of pile-up on the f_T variable at the highest luminosities.

To put these results in context, the results published in [1, 2] assume that BSM Higgs scenarios, such as the MSSM and triplet Higgs models, can be observed with asymmetric tagging with a prescale of about 5. Depending on the exact rejection factor provided by the f_T variable, we have demonstrated that a prescale of between 1.5 and 7 would reduce the rates to the 2 kHz level. AFP members plan to be actively involved in the Phase I L1 calorimeter trigger upgrade in order to guarantee these capabilities.

2.2.2 Level 1 bandwidth for alignment

The L1_2MU6 trigger (2 muons with $p_T > 6$ GeV) is a major physics trigger for ATLAS and is likely to be unprescaled up to a luminosity of several 10^{33} $cm^{-2}s^{-1}$ and have only a modest prescale (3 to 5) at 10^{34} $cm^{-2}s^{-1}$, where its unprescaled L1 rate is 15kHz. This trigger will be used by AFP to obtain an exclusive dimuon calibration sample. At L2 and EF, if the standard dimuon trigger were to be prescaled, we would add a parallel trigger that would complement the standard muon rejection by requiring that the two muons are back-to-back azimuthally and that there is a proton with appropriate momentum in the AFP detectors. Over the course of a typical high luminosity store, an unprescaled trigger would give us over 2000 calibration events. As several hundred such events would suffice for calibration purposes, we can afford a modest prescale at high luminosity.

2.3 Quantum number determination

If a Higgs signal is observed in the central detector, it will be important to confirm its properties, especially the quantum numbers. There are two approaches to determine the quantum numbers – either by production or decay. The methods are summarised in the table below.

Channel	**Quantum number determination due to production mechanism**
CEP	If the Higgs is created via central exclusive production, then selection rules require it to be $J^{PC} = 0^{++}$.
VBF	Some channels have been demonstrated - T. Plehn, D. Rainwater, D. Zeppenfeld.
	Quantum number determination from analysis of Higgs decay
CIP	H-> ZZ angular correlations for quantum numbers possible for a heavy Higgs. Observation of H-> $\gamma\gamma$ requires that C must be positive and J = 0.

AFP offers a complementary approach to the few existing standard approaches in central inclusive production. The CEP technique is likely to work with standard model or BSM production of Higgs bosons. In addition, CEP measures the Higgs vector boson couplings and the Higgs quantum numbers as two independent measurements, whilst in other approaches the two determinations and their interpretations are interconnected.

A more detailed note is given in the Appendix.

2.4 Higgs Signal to Background Studies

We have been augmenting previous internal AFP studies on the Higgs physics case using ATLFAST with the ExHuME Monte Carlo and various Monte Carlo samples with either full simulation if available, or ATLFAST if the full simulation samples did not exist. A detailed note is in preparation, and we provide a summary of the important points here. We have studied two decay modes of the Higgs boson, $H \to b\bar{b}$ for M_H = 120 GeV and $H \to WW^*$ in the semi-leptonic channels with $WW^* \to l\nu jj$ and M_H= 160 GeV (with l = e or μ). We used the latest acceptance calculations as outlined in Sec. 4, with the active area of the detector at 220 m (420 m) located at 2.5 (4 mm) from the beam, giving an acceptance of about 20% each for 220-420 and 420-420 configurations at M_H = 120 GeV, and 40% for 220-420 at M_H= 160 GeV, with only a small acceptance for the 420-420 configuration.

We did not study the trigger efficiency of $H \to WW^*$, assuming that ATLAS will develop a highly efficient unprescaled trigger for this critical channel. If that turns out not to be the case, we could add a 220 m proton tag to allow us to retain the events in the 220-420 configuration which comprise most of the high mass acceptance.

In both decay channels, various sources of background were studied, including backgrounds from other exclusive processes and overlap backgrounds, which fake the exclusive signal through the combination in one bunch crossing of three separate interactions that contain two opposite arm protons and a central hard scatter. The former background type scales with luminosity in the same manner as the exclusive signal, while the fake backgrounds grow with the square of the number of interactions. A number of efficient "exclusivity'' cuts to suppress overlap backgrounds were developed. The important tracking exclusivity cut was validated using full detector simulation. The exact cut values become somewhat higher with full simulation, but it is possible to maintain high signal efficiency with large background rejection. Recent advances in low p_T tracking have not yet been incorporated into our studies, but will provide additional rejection of background for a fixed signal efficiency. In addition to topological variables, a global background reduction factor of 20 at lower luminosity and 15 at high luminosity is provided by the use of fast timing detectors.

For a standard model Higgs, we would expect to collect about 1.3 candidate events for a recorded integrated luminosity of 30 fb^{-1} in the $H \to b\bar{b}$ channel for M_H= 120 GeV (with a 50% trigger efficiency included but not the effect of prescales) and about 2 candidates in the semi-leptonic mode at M_H= 160 GeV. For the $H \to b\bar{b}$ channel the signal to background ratio is kept close to unity for instantaneous luminosities of up to 2 x 10^{33} $cm^{-2}s^{-1}$, while the background situation for $H \to WW^*$ (studied in detail for the semi-leptonic muon decay mode) is more favourable giving a signal to background ratio close to unity for instantaneous luminosities up to about 10^{34} $cm^{-2}s^{-1}$. Details of the running scenario thus become important - as the luminosity increases, prescales in the $H \to b\bar{b}$ channel reduce event yields, and there is a quadratic growth in the overlap background. Consequently there is a larger significance for a data sample collected at low luminosity compared to an equivalent sized sample collected at higher luminosity. Clearly, the dependence of significance on luminosity can be mitigated by optimized analyses that gradually tighten cuts as a function of luminosity, modestly reducing signal efficiencies at high luminosity in order to maintain reasonable signal to background ratios.

While the heavier mass Higgs is not very sensitive to the detector position - varying by 20-30% over a reasonable range of positions - we observe that if the 220 m detectors are located 3 mm or further from the beam, the acceptance of the 220-420 configuration is small, and only 420-420 events give a reasonable acceptance. However, 0.5 mm is a significant distance for the 220 m detectors in terms of the primary beam width, and we expect that the 2.5 mm position is well within the shadow of the collimators, and should be obtainable.

Our current understanding after detailed studies is consistent with the previous generator-level studies, namely that under realistic assumptions, the enhanced cross sections predicted by BSM Higgs models are required to observe the Higgs Boson in the $H \to b\bar{b}$ channel, while, if the Higgs is heavier, the SM Higgs is observable in the *WW** channel. As discussed in Sec. 2.3, the simple observation of a Higgs signal establishes its quantum numbers, and only a few events are needed for a precise mass measurement. In addition to a sufficiently large data sample, the observation of a 120 GeV Standard Model Higgs would require further improvements in the trigger capabilities combined with improved background rejection, both of which may be possible given experience operating the detectors. We also note that the *WW** cross section is only a slow function of Higgs mass - the cross section at 140 GeV is only reduced by 20% relative to 160 GeV - and that tau

decay modes and dilepton channels will give further enhancements to the significance. Combining channels and applying realistic running scenarios has the potential to extend our Standard Model Higgs reach to 130 GeV and possibly below.

2.5 Possible Running Scenario

Assuming all bunches have the same initial population and each bunch decays exponentially with lifetime τ =15 hours with $L = L_0 \exp(2t/\tau)$. If each store started with $L_0 = 10^{34}$ $cm^{-2}s^{-1}$, and lasted for 15 hours, this would correspond to a total of 45 fb^{-1} per year assuming an LHC year of 10^7 seconds. A plausible ATLAS running scenario would involve commencing with a one hour run while the AFP detectors were being inserted. This could be followed by a two hour run and then three four hour runs. The table below shows the integrated luminosity obtained in bins of instantaneous luminosity assuming that 300 fb^{-1} were collected in this manner. This type of scenario is more realistic compared to the equivalent integrated luminosity concentrated at 10^{34} $cm^{-2}s^{-1}$. Due both to the lower prescale factors and the lower relative background for smaller instantaneous luminosity this scenario improves the performance of the AFP detector. If more than 2-3 kHz were allotted at low luminosity, it would be possible to retain a larger fraction of the 420-420 events.

Hours into store	0-1	1-3	3-7	7-11	11-15
Integrated Luminosity (fb-1)	42	73	97	55	33
Instantaneous Luminosity (10^{34})	1.0	0.88	0.67	0.39	0.23
Average Lum (10^{34})		0.78	0.54	0.32	0.2
220-420 with f_t kHz (prescale)	-	2.2 (1)	1.3(1)	0.4(1)	0.2(1)
420-420 with f_t kHz (prescale)	-	-	1.8(10)	2.8 (5)	2.4(2)
Total Rate (kHz)	0	2.2	3.1	3.2	2.6

We estimate that this would give an improvement on the significance ($S/\sqrt{B}$) of at least a factor two compared to a constant luminosity of 10^{34} $cm^{-2}s^{-1}$ which is the assumption used in previous physics notes.

3. Other trigger issues – detector and latency

"Trigger from the Si-detector. In order to provide a LVL1 trigger from the Si-detector an R&D program is needed"

"The LVL1 latency for the signals from the 220 m stations seems to be close to or even over the ATLAS limit. A detailed study on this item is needed, in order to prove that the AFP detector can provide a trigger signal".

3.1 Level 1 trigger from 220 m

We have decided to use a quartz fibre Cerenkov detector as our baseline L1 proton trigger system. A detailed note on this system is attached in the Appendix. The review committee was correct to be concerned about the latency. After detailed work, dependent on the electronics, a latency of 1850 to 1960 ns is found. The note should be read to appreciate the details that went into these calculations. This should be compared with the ALFA TDR value of 1940 ns. The conclusion is that we can design and build a system to keep within a latency time of 1900 ns. Dedicated air-core signal cables will have to be installed following a similar route as the ALFA cables. Since the June 22nd meeting, we have had follow-up discussions on latency matters with D. Berge, H. Wilkens, and T. Wengler. There is a complicated relationship between latency, L1 calorimeter buffer size and deadtime. There will have to be continuing contact between AFP and the trigger/DAQ people to integrate a trigger from 220 m into the L1 trigger.

3.2 Level2/HLT trigger comment

"No L2/HLT simulation was shown. Level 2 trigger assumes that there is a central detector primary vertex resolution comparable to what one gets from timing. This is not known to be true. "

We note that the estimated L2 vertex resolution of 800 μm is small compared to the estimated 2 mm resolution from the timing detectors, and will thus not significantly degrade our timing rejection. Given a 2 kHz L1 rate, we would plan to have a factor of 50 to 100 rejection at L2 and reduce the total rate to a couple Hz at the Event Filter (EF). At L2 we will have the full kinematic information available for the 220 m and 420 m protons; the strategy would be to require that the di-jet system mass and rapidity is consistent with the proton measurements and to apply a vertex matching cut using proton time-of-flight information. At the EF level, we will improve these exclusivity cuts in addition to applying central tracking cuts to further reject the non-exclusive backgrounds. In conclusion, we do not anticipate any HLT trigger issues for AFP Higgs physics.

4. Collimators at 220 – acceptance studies.

"Collimators: this can be a very critical issue, even more after the 2013 shut-down. The collimator in front of the station at 220m (TCL) will very seriously limit the acceptance for the 220 meter station if needed to be closed to 10 or 15 sigma"

The LHC collimation system includes two collimators on both sides of ATLAS, located on the outgoing beams trajectory, at about 140 and 190 m from the IP, labelled as TCL4 and TCL5, respectively. Such collimators are designed to protect superconductive elements of the LHC from 'physics debris' generated at IP1. Preliminary studies by machine physicists suggest that they will be needed at luminosities larger than a few 10^{33}. Detailed studies to determine the optimal collimator settings have not been completed. The document in which the installation of the TCL5 collimator was first proposed (J.B. Jeanneret and I. Baichev, LHC-Project-Note-208) asserts that those collimators cannot be closed to less than 10 σ_x (to avoid interference with the IR3 and IR7 cleaning system) and that 15-20 σ_x is enough to protect the LHC long straight section and dispersion suppressor. This does not exclude the possibility that larger aperture settings are acceptable.

While it has been shown that collimator operation does not affect the acceptance of the 420 m detectors, the TCL5 collimator can compromise the acceptance at 220 m. We are studying two possible alternative solutions:

1) the displacement of TCL5 downstream of AFP220 provides comparable protection to the LHC given appropriate settings on TCL4, while preserving the 220 m acceptance.
2) the relaxation of the TCL5 settings to allow physics at 220 m combined with the installation of a new collimator downstream of AFP220 to provide additional machine acceptance.

Using the beam optics around IR1, we calculated the collimator aperture necessary to intercept all protons with a momentum loss w.r.t. p_0 = 7 TeV, $dp/p_0 > p_{cut}$, for different locations of the collimator. Figure 4.1 shows the results for the LHC straight section on the right side of ATLAS. The location of the two existing collimators (TCL4 and TCL5) and a favourable position for a new collimator (TCL6) downstream of AFP220 are included in the figure. As an example, in order to intercept all protons with $dp/p_0 > 0.05$, a collimator at 190m (TCL5) needs to be set at about 20 sigma (~5.8 mm at this location), whereas at about 225m (TCL6) the settings can be relaxed to more than 80 sigma (~5.7 mm at this location). In general, the location of TCL6 looks more convenient than TCL5 for cleaning protons that are potentially lost in the dispersion suppressor. Of course one needs to properly set the other one (in case it is decided to move TCL5 at the new location) or two collimators (in case it is decided to keep TCL5 and add a new TCL6) to protect the region between Q5 and Q6.

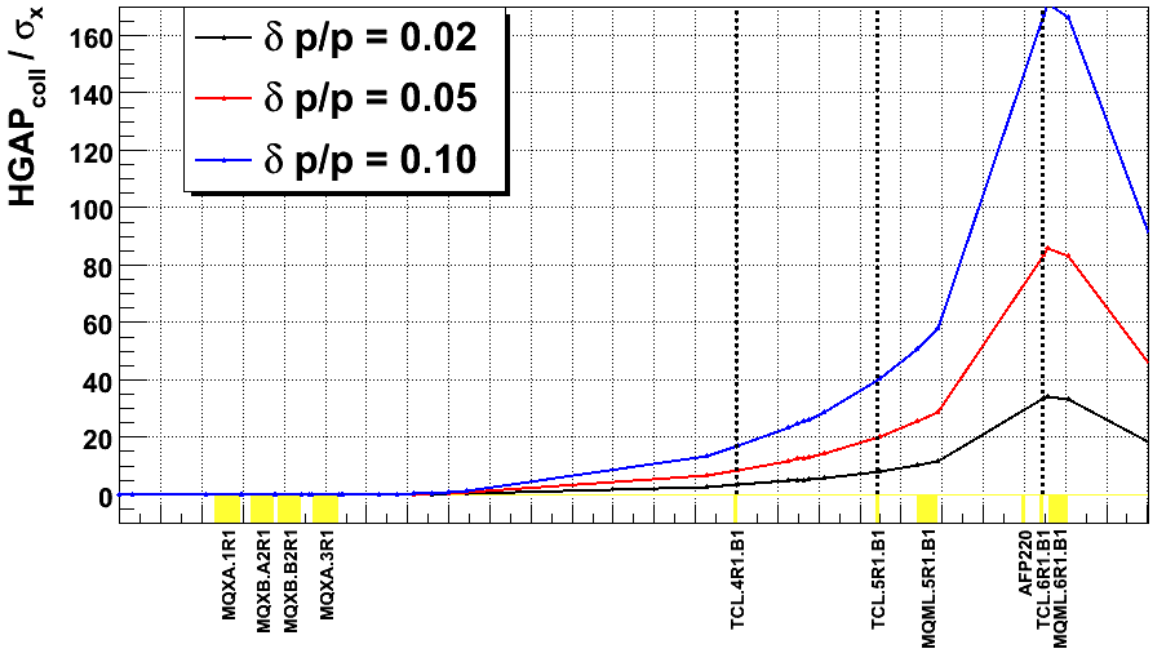

Figure 4.1: Required collimator half gap as function of collimator location, for three different momentum cuts.

In order to confirm this 'argument-in-principle', loss maps of proton samples have been generated using DPMJET and MADX for different settings of the two collimators. These show very good agreement with published results (Jeanneret-Baichev) in terms of integral and peak losses in the dispersion suppressor.

Forward protons generated by p-p collisions are tracked until they are intercepted by a machine element. Any aperture limitation, including collimators, is treated as a black body absorber. Loss maps are normalised to the nominal LHC luminosity of 10^{34} $cm^{-2}s^{-1}$.

Figure 4.2 shows the loss maps results for 3 different cases:

1) No collimator installed (black dashed line):
some super-conductive elements approach or exceed the quench limit, e.g. Q5.

2) TCL4 at 30 σ, TCL5 not installed, TCL6 at 40 σ (green solid line):
losses immediately downstream of TCL4 are almost eliminated,
peak losses in Q5 region are reduced by an order of magnitude,
integrated losses on in the MB8-MB9 region are strongly reduced

3) TCL4 at 30 σ, TCL5 at 50 σ, TCL6 at 40 σ (red dash-dotted line):
in addition to case 2, losses on Q5 are not only reduced but eliminated

These results are completely consistent with the 'argument-in-principle' presented above. We have confirmed by direct tracking studies that the collimator settings of case 3 (and consequently also case 2) have no deleterious effects on the 420-420 acceptances or on the 420-220 acceptances up to centrally produced masses of about 250 GeV. At higher masses up to 700 GeV, a small loss of acceptance of up to 20% is seen. At this stage, both case 2 and 3 can be considered as acceptable for machine protection.

The uncertainties of these simulations arise due to the accuracy of the p-p interaction model, real machine imperfections that may affect the tracking, and the effect of secondary showers generated by proton losses. These are all expected to be second order effects which will not drastically change the general conclusions.

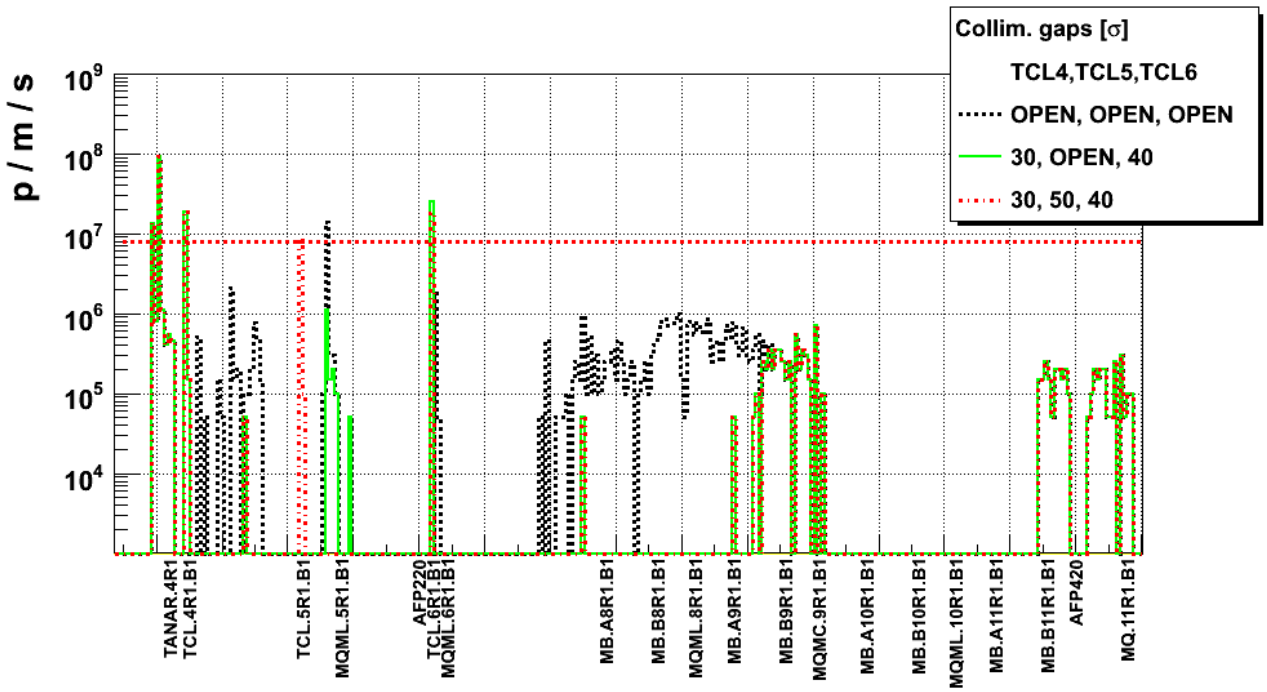

Figure 4.2: Loss maps of forward protons on the right side of ATLAS, for different collimator settings. The horizontal red dashed line is an estimation of the quench limit for super conducting magnets.

The possible interference between AFP physics and the LHC collimation along IR1 has been discussed in a CERN BE-ABP meeting where our loss maps results and proposals were presented. The minutes of such discussion can be found at:

http://ab-dep-abp.web.cern.ch/ab-dep-abp/LCU/LCU_meetings/2009/20090324/agenda2.html

It has been already been agreed with the relevant machine people that we will present the latest results and proposals at the LHC collimation working group.

The AFP proposal and possible interference with collimation has been also discussed in a recent review of the LHC collimation. AFP concerns have been presented as an example of possible requirements by the experiments to the LHC machine in visage of the collimation system upgrade. The relevant presentation can be found at:

http://indico.cern.ch/materialDisplay.py?contribId=10&materialId=slides&confId=55195

An updated mass acceptance is shown in Figure 4.3.

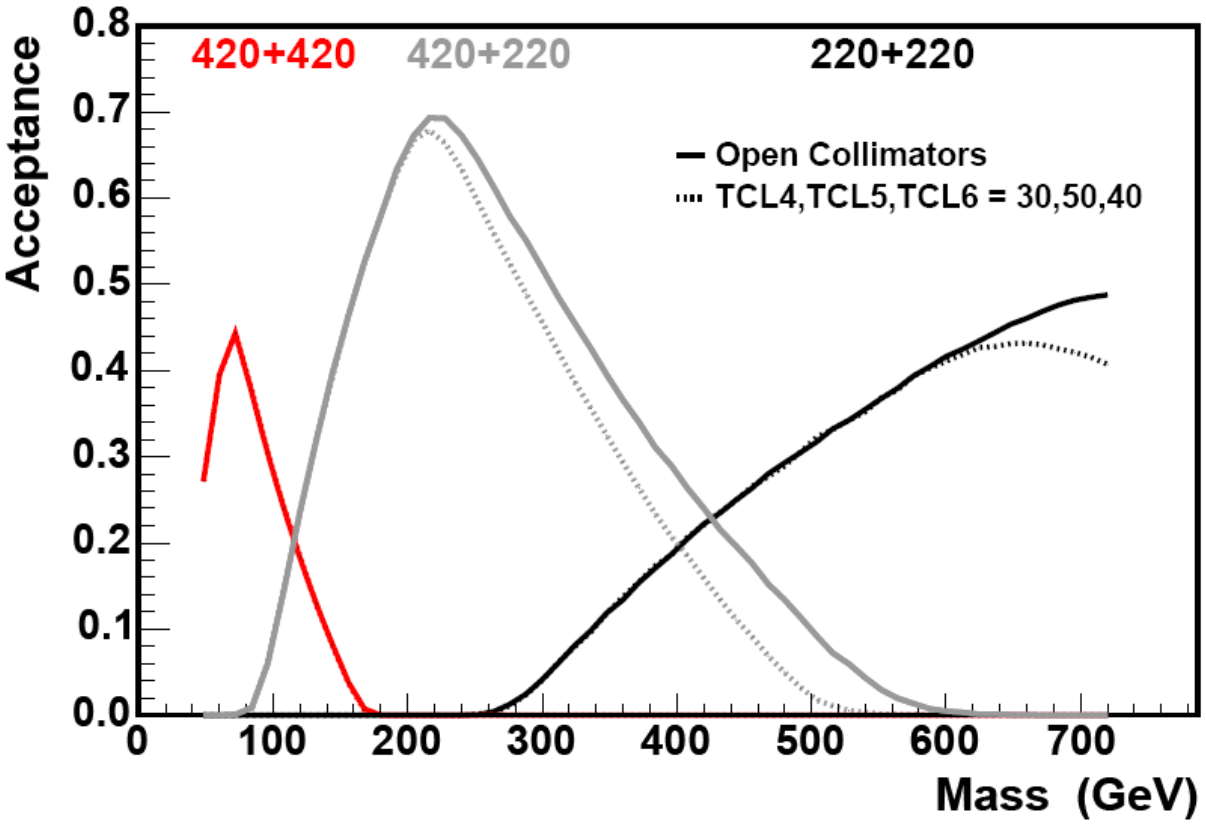

Figure 4.3. Updated mass acceptance plot for 220 and 420 m.

In conclusion, a solution is possible that works for both the LHC and AFP. It will be important to continue to maintain our excellent contacts with our colleagues in the machine division.

5. Detector Related Questions

“

a) ***the phototube lifetime for the timing detectors is critical. A phototube that has sufficient lifetime may exist commercially at some time but does not today. In order to match the requirements many separate improvement factors are needed. If many of them will be close to (but not at) the predictions, there will not be enough improvements.***

b) ***The innermost chip will die after a year. There is no plan on how to replace it. “***

“The project is well advanced, but still some work is needed in some areas like for example the design of the stations at 220 m or the trigger scheme”

5.1 MCP-PMT Lifetime

There has been considerable effort to define an R&D programme to improve the MCP-PMT lifetime. Measurements show that we can operate the phototubes at reduced gain. However, a factor of about 50 improvement in the lifetime is still required to operate at the highest luminosity. We are confident that the combination of an optimized detector design along with a development programme pursued in collaboration with key manufacturers will solve this problem on a two to three year time scale. The R&D programme, already in progress, is described in detail in the Appendix.

5.2 Silicon Tracker

The 3D sensor is radiation hard to 1-2 10^{16} charged particles per cm^2. However, the FE-I3 ATLAS pixel readout chip which uses 0.25 micron technology is radiation hard to ~$2x10^{15}$ charged particles per cm^2 or ~50 Mrad. There are two possible solutions.

i) The dose is highest in very narrow vertical band. By moving the sensors up and down by 1-2 mm the dose can be evened out. This technique was used with charge coupled devices in NA32. This is described in more detail in the Appendix. This technique would give a factor three improvement in the lifetime, or around 3 years at L= 10^{34} $cm^{-2}s^{-1}$. This is an additional specification for the mechanical design. It has been discussed with the mechanical engineers and can be implemented.

ii) The FE-I4 chip is being developed for the IBL project. This chip is approximately double the size of the FE-I3 chip vertically and horizontally. It uses 0.13 micron technology and is known to be a factor of four more radiation tolerant than the FE-I3. The first chips will be available in late 2010 with IBL modules expected at the end of that year. This chip is well-matched to the hit pattern expected in the 220 m detectors and would simplify the superlayer design. A common superlayer design for 220 and 420 also has advantages. We are in close contact with the R&D effort for the IBL project, and may use this readout chip if progress is good in 2010.

The combination of these two solutions would give a ten year lifetime at L = 10^{34} $cm^{-2}s^{-1}$.

Mechanical engineers have drawn up the 220 m design using the FE-I3 readout chip based detector. It is based on the 420 m design. Figures are shown in the appendix.

Note that the silicon trigger detector at 220 m has been replaced with a quartz bar readout using a MCP-PMT. See Section 3.1.

6. Safety

"Safety: safety issues associated to the AFP detectors for the machine and the experiment could be critical for the project (see for example the recent problems at Tevatron)"

Addressing safety issues associated with AFP installation and operation is a continuing process that will proceed through the TDR stage and during operation. We note that bi-monthly technical integration meetings between FP420 members from ATLAS and CMS and CERN experts in vacuum, cryogenics, engineering, etc., have been taking place for several years, in part to ensure a safe and seamless integration of the proton detectors and connection cryostats into the LHC. Safety issues will managed by a Safety Review Panel which will include LHC machine physicists and AFP physicists and engineers. It has been agreed that a nominee from the ATLAS management will join this panel. In addition, AFP and CMS/FP420 have agreed to jointly perform a Risk Review during the TDR stage. This will be similar to the one performed for the LHCb VELO which is also closely integrated with the LHC.

References

[1] M. G. Albrow et al. [FP420 R&D Collaboration], "The FP420 R&D Project: Higgs and New Physics with forward protons at the LHC," http://arxiv.org/abs/0806.0302, accepted by J. Inst.

[2] "Searching for the Higgs Boson at Hadron Colliders using the Missing Mass Method," M. G. Albrow and A. Rostovtsev, arXiv:hep-ph/0009336.

"Diffraction as a CP and lineshape analyzer for MSSM Higgs bosons at the LHC," J. R. Ellis, J. S. Lee and A. Pilaftsis, Phys. Rev. D 71, 075007 (2005).

"Detecting Higgs bosons in the bb decay channel using forward proton tagging at the LHC," B. E. Cox, F. K. Loebinger and A. D. Pilkington, JHEP 0710 (2007) 090.

"Studying the MSSM Higgs sector by forward proton tagging at the LHC," S. Heinemeyer, V. A. Khoze, M. G. Ryskin, W. J. Stirling, M. Tasevsky and G. Weiglein, Eur. Phys. J. C 53 (2008) 231.

" Reinstating the 'no-lose' theorem for NMSSM Higgs discovery at the LHC," J. R. Forshaw, J. F. Gunion, L. Hodgkinson, A. Papaefstathiou and A. D. Pilkington, JHEP 0804 (2008) 090.

"Searching for the triplet Higgs sector via central exclusive production at the LHC," M. Chaichian, P. Hoyer, K. Huitu, V. A. Khoze and A. D. Pilkington, arXiv:0901.3746 [hep-ph].

"Detecting the Standard Model Higgs Boson in the WW decay channel using forward proton tagging at the LHC," B. E. Cox, A. De Roeck, V. A. Khoze, T. Pierzchala, M. G. Ryskin, I. Nasteva, W. J. Stirling, M. Tasevsky. Eur. Phys. J. C 45, 401–407 (2006).

[3] Talk by S. Heinemeyer at EDS 2009 – see CERN Indico page.

APPENDIX

1) **Central Exclusive Production and Higgs quantum numbers.**
2) **Level 1 triggering for $H \to b\bar{b}$.**
3) **Conceptual design and latency for a trigger detector at 220 m.**
4) **Plans to Address Phototube Lifetime Issue for AFP Fast Timing Detectors**
5) **AFP Silicon Trackers – Update July 2009**

Central Exclusive Production and Higgs quantum numbers

P J Bussey, M Campanelli and A D Pilkington

The process of central interest in our work is central exclusive Higgs production. Measuring both outgoing protons provides a narrow mass resolution for any produced resonance, which can augment central Higgs mass measurement and helps to improve the signal/background ratio with respect to inclusive production. In addition, the observation of the Higgs in this channel provides important information on its quantum numbers.

In general, the quantum numbers of a state may be studied by studying (a) its production process, or (b) its decay products. For the CEP Higgs, we employ approach (a). The production of any particle from two identical hadrons implies that its C-parity is positive. Resonance production in CEP very much favours the set of quantum numbers $J^{PC} = 0^{++}$ [1]. Consequently, the observation of CEP Higgs with a cross section roughly in agreement with prediction implies that the 0^{++} state is at least strongly present. In principle the azimuthal distribution of the protons can provide further information [2].

To evaluate the merits of this method, we consider the measurements possible in inclusive production channels: The only method using the production process so far advocated is by Zeppenfeld et al [3]. The vector boson fusion (VBF) channel is employed and the angular correlation of recoil jets is studied. It was shown that the tensor structure of the SM coupling,and hence the spin/parity, could be determined with 100 fb^{-1} (per LHC experiment) in the tau-tau channel for a 120 GeV Higgs. An ATLAS study of this channel [4] concluded that the purely anomalous couplings (e.g. CP negative) could be excluded at 5σ (2σ) for a 160 (120) GeV Higgs boson given 10 (30) fb^{-1}. Effects of pile-up and higher order jet production were not yet included.

All other methods of extracting the quantum numbers of the Higgs utilize information from the decay products, in particular their angular correlations. A decay into two identical particles again tells us that C = +. The Higgs decay into two photons would therefore rule out negative C at the same time as it rules out J = 1, but leaving the parity undetermined.

Extracting the quantum numbers will be very hard for a statistically difficult channel such as H -> $\gamma\gamma$ since the angular properties of the large background must also be very well understood. The major other possibility that has been discussed is the decay H -> ZZ -> 4 leptons [5]. It has been shown that, above $2m_z$, the angular distribution obtained from the lepton measurements can be used to obtain the spin and parity of the SM Higgs boson. Below the $2m_z$ threshold, it has been shown that the threshold effects and angular correlations can be used, but in both cases the required luminosity is relatively large (100-300 fb^{-1}). Furthermore, in the latter case ($m_H < 2m_z$), sensitivity was demonstrated for a 150 GeV Higgs boson. The lower branching ratio for a lower Higgs mass would make this channel more difficult for statistical reasons.

The requirement of detecting the entire final state and the need to understand backgrounds very well can make standard approaches challenging, particularly if different channels need to be combined. In a general review, Djouadi and Godbole expressed confidence that 300 fb^{-1} of LHC luminosity could measure certain of the SM Higgs properties, in the channels mentioned above, while suggesting that precise Higgs quantum number determination might have to wait for the ILC [6]. One aspect of all the inclusive approaches is a heavy reliance on the coupling to W's and Z's. It is a feature of extended or non-standard Higgs sectors, such as the MSSM and triplet models, that a Higgs boson can have reduced branching ratio, and even suppressed coupling, to the vector bosons. It is exactly these scenarios, with the corresponding increase in coupling to b's, tops etc, that AFP can measure very well. Furthermore, there are regions of the MSSM parameter space in which one (or both) of the Higgs bosons can be approximately degenerate in mass to the pseudo-scalar. In this case, AFP projects out only the scalar particle. In addition, Ellis et al. have suggested that AFP-based measurements could probe CP violation in the MSSM Higgs sector [7]. Finally, in

the NMSSM it has been demonstrated that AFP could measure the problematic H -> aa -> 4τ decay channel, which can dominate for certain, natural, parameter choices; in this channel, the ATLAS central detector on its own has been claimed to have discovery potential but with low statistics [8].

In summary, AFP offers a complementary approach to the small number of standard approaches in central inclusive production, and an approach that is especially likely to work with regard to the non-standard model production of Higgs bosons. We note also that CEP measures the Higgs vector boson couplings and the Higgs quantum numbers as two independent measurements, while in other approaches the two determinations and their interpretations are interconnected.

References

[1] V. Khoze et al., Eur. Phys. J. C24 (2002) 581
[2] V. Khoze et al., hep-ph/0307064; S. Heinemeyer et al arXiv:0801:1974
[3] T. Plehn, D. Rainwater, D. Zeppenfeld, Phys. Rev. Lett. 88:051801,2002
[4] C Ruwiedel, M Schumacher, N Wermes, ATLAS note: SN-ATLAS-2007-060; Eur. Phys. J. C51 (2007) 385
[5] A. Rosca Rom. Rep. Phys. 59 (2007) 987
[6] A Djouadi and R Godbole, arXiv 0901.2030 [hep-ph]
[7] J. R. Ellis, J. S. Lee and A. Pilaftsis, Phys. Rev. D 71 (2005) 075007 [arXiv:hep-ph/0502251].
[8] Investigation of the ATLAS Discovery Potential for NMSSM Higgs bosons.
I. Rottlaender and M. Schumacher, ATL-COM-PHYS-2008-149.
Development of a Benchmark Parameter Scan for Higgs Bosons in the NMSSM Model and a Study of the Sensitivity for H –> aa -> 4τ in Vector Boson Fusion with the ATLAS Detector - Rottlander, Iris et al - CERN-THESIS-2008-064)
Rottlander and M Schumacher, ATL-PHYS-INT-2009-001 the bibliography

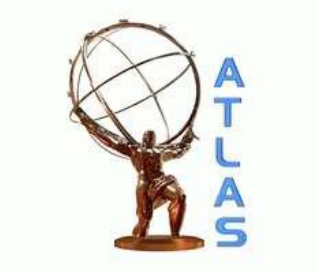

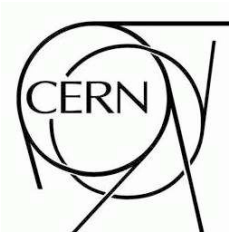

Trigger strategies for central exclusive $H \to b\bar{b}$ studies with the AFP detector

G. J. A. Brown[1], M. Campanelli[2], A. Kupco[3], A. D. Pilkington[1], M. Tasevsky[3]

[1] *School of Physics and Astronomy, University of Manchester, Manchester, M13 9PL, UK*
[2] *Department of Physics and Astronomy, University College London, London, WC1E 6BT, UK.*
[3] *Institute of Physics of the AS CR v.v.i., Na Slovance 2, CZ-182 21 Praha 8, Czech Republic.*

Abstract

The ATLAS Forward Proton (AFP) upgrade proposes to install proton detectors at 220 m and 420 m either side of the ATLAS interaction point, turning the LHC into a giant magnetic spectrometer. The physics motivation for this upgrade focuses on final states in which the colliding protons remain intact, allowing a full reconstruction of the event, even in the forward region. One such process is the production of the Higgs boson in the central exclusive channel and tagging the outgoing protons allows the possible extraction of the Higgs quantum numbers, mass and couplings regardless of the decay channel. Studying this exclusive production channel for the presently favoured low Higgs mass depends on the possibility of efficiently triggering, up to the highest luminosities, on a pair of relatively soft jets coming from the decay of b quarks or τ leptons. As jet triggers will inevitably be heavily pre-scaled, even at modest luminosities, it is essential to make a coincidence betweeen information from the tagging detectors and the central system as early at Level 1. In this note, we describe some possible solutions that result in an efficient low-mass $H \to b\bar{b}$ trigger with AFP.

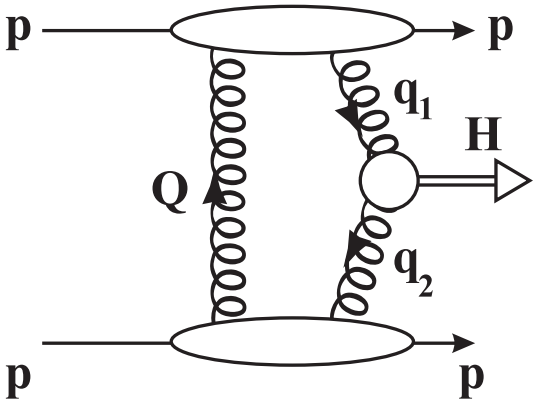

Figure 1: The central exclusive production of Higgs bosons at the LHC.

1 Introduction

The importance of the central exclusive production (CEP) mechanism to study the Higgs boson properties has been already discussed in many dedicated papers [1, 2, 3]. The Higgs boson is produced by gluon-gluon fusion, but the protons remain intact due to the presence of a screening gluon as shown in Figure 1. The final state therefore consists of a Higgs boson, two outgoing protons and no other hadronic activity. Only scalar particles can be produced as resonances in this channel. We do not go into further details, but remark that this channel has often been described as the possibility of performing at the LHC some of the measurements only believed possible at a future Linear Collider.

It is also worth mentioning that, although central exclusive Higgs production cannot be considered as a discovery channel due to the larger luminosity required with respect to more standard channels, the mass measurement obtained could be much better. In this case, the Higgs mass would be calculated from the very well measured momentum of the two protons detected in the AFP detectors, exploiting the fact that the Higgs boson is produced *exclusively*. The AFP proposal is to build four tracking stations located at 220 m and 420 m on both sides of the ATLAS interaction point (IP). The detectors will be capable of measuring both the position of a proton with respect to the beam and the time-of-flight of each proton from the interaction point. Further details regarding the AFP detector can be found in [3]. Finally, it should be noted that, in addition to precision Higgs boson measurements, there is a wide range of electroweak physics studies possible with the AFP detectors. These include anomalous gauge boson couplings and supersymmetry measurements and can be studied using standard ATLAS leptonic triggers.

In this note, we determine a trigger strategy to retain central exclusive $H \rightarrow b\bar{b}$ events. As we will see in the following, the knowledge of the approximate value of the Higgs mass can be used to reduce the rates at trigger level, keeping good efficiency for the signal. The layout of the note is as follows: In section 2, the ATLAS Level 1 (L1) calorimeter trigger system is discussed, both in relation to its present configuration and proposed upgrade. In section 3, the L1 trigger capability of the proposed AFP detectors at 220m will be discussed. In section 4, the trigger efficiency for signal events is discussed. Finally in section 5, the background rates for a variety of trigger strategies are presented.

2 The ATLAS L1 Calo system: present configuration and proposed upgrades

The ATLAS L1 Calorimeter trigger is composed of a central region, plus two forward-backward regions. Central and forward calorimeters are seen by the system as two independent detectors. The boundary between the central-forward regions is set at a pseudo-rapidity value of 3.2, i.e. the physical boundary between the forward calorimeter (FCAL) and the hadronic endcap.

At present, jets are reconstructed in towers of 0.8×0.8 in the $\eta-\phi$ plane. However, detailed information (E_T, η, ϕ) is not propagated to the central trigger processor (CTP) for bandwith occupancy reasons and therefore cannot be used for the trigger decision. The only information currently available to define L1 jet trigger items is the number of jets passing a given transverse energy threshold (separately for the central and forward regions). For the 2009-2010 data taking, to keep the system as simple as possible, it was decided that only inclusive single jet signatures are used - the only exception is the forward di-jet (2FJ18) trigger that requires two jets in the forward calorimeters above an E_T threshold of 18 GeV.

At the time of the AFP detector installation, a substantial upgrade of the L1 calorimeter trigger system is likely to be operational [4]. The main improvement would be an increase of the bandwith, allowing the use of the E_T and topological information of each individual jet in the L1 processing. The processing itself would require a new *global merger* processor, which would allow the definition of new trigger quantities based on the leading jets in the event. This new processor is foreseen to be part of the trigger upgrade and we will present trigger rates that utilize this topological information in section 5. It is also foreseen that the granularity would be improved by a factor two and so it is likely that η and ϕ information for each jet will be available in discrete values of size 0.4×0.4. Finally, quantities such as di-jet mass could be calculated using the global merger processor. We do not consider such an option in this note, but draw attention to the fact that this could allow a further reduction in the L1 rate.

3 Trigger considerations for the detector station at 220 m

The jet (and di-jet) L1 trigger items will be heavily pre-scaled even at moderate instantaneous luminosities. In order to keep a relatively high efficiency for the Higgs search, we need to impose a coincidence between the two jets in the central region and a tagged proton in the forward detector. To get the best mass resolution, we have to require also that the other proton is detected in the opposite side in the 420 m station (for the light Higgs case), but unfortunately this detector is too far to be included in the Level 1 trigger information. In fact, the maximum value of the L1 latency for a complete trigger decision is 2500 ns[1)]. This means that the signal from each sub-detector has to reach the CTP within 1900 ns, since about 600 ns are needed to take a decision and propagate it to the various sub-detector systems. The time-of-flight of the proton from the interaction point to the 420 m station, plus the time it would take for a signal, even travelling at the speed of light, to reach the CTP is much larger than the 1900 ns limit. On the other hand it is, in principle, possible to trigger on protons tagged in the detector stations at 220 m from the interaction point. The present baseline design for the 220 m trigger system foresees the use of a quartz bar detector, shaped to optimize signal/background rejection, read out by an optical fibre. The fibre would be read out by an MCP photomultiplier, amplified, and the signal accepted if it passes the threshold of a constant fraction discriminator. After a local

[1)] The current latency is somewhat smaller than this.

coincidence logic, the signal would be sent to the CTP using an air-core cable similar to what is used by the ALFA detector [5]. Details of the proposed system are discussed in a separate note [6].

The main contribution to the L1 rate for our *di-jet plus proton* trigger comes from the coincidence, in the same bunch crossing, of a di-jet event and an event that produces a forward proton, mainly coming from single-diffractive or non-diffractive scattering, within the AFP acceptance.

The probability that in N proton-proton interactions there are k events producing a forward proton is a binomial,

$$B(N,k) = \binom{N}{k} (2\varepsilon)^k (1-2\varepsilon)^{N-k}, \tag{1}$$

where ε is the fraction of events at the LHC that have a forward proton within the acceptance of the 220 m detector station. A proton is observed for $k \geq 1$, so the probability of a proton 'hit' at 220 m is given by

$$B(N) = \sum_{k=1}^{N} B(N,k) = 1 - (1-2\varepsilon)^N, \tag{2}$$

which is valid for exactly N interactions. Assuming that there are, on average, μ interactions per bunch crossing, the probability of a forward proton within the acceptance of the detector stations at 220 m is

$$P = \sum_{N=0}^{\infty} P_\mu(N) B(N) = 1 - e^{2\mu\varepsilon} \tag{3}$$

where $P_\mu(N)$ is the poisson distribution, i.e.

$$P_\mu(N) = \frac{\mu^N}{N!} e^{-\mu}. \tag{4}$$

If we also require that a hard scatter is present, we have to replace $P_\mu(N)$ with

$$P'_\mu(n) = \frac{P_\mu(N+1)}{P_\mu(1)}. \tag{5}$$

In the end the combined probability of having a tagged proton and a hard event is

$$P' = 1 - \frac{1}{1-\varepsilon} \frac{e^{-\varepsilon\mu} - e^{-\mu}}{1-e^{-\mu}}. \tag{6}$$

Note that a change in the expected vaue of μ can have a large effect on the probability of having a hard scatter and a forward proton tag in the same bunch crossing. This means that the rate of a trigger based on a forward proton at 220 m from the IP has more than a linear dependence on the average number of interactions in each bunch crossing, and hence the luminosity.

The key to reducing this background in the L1 trigger is to reduce ε, i.e. the acceptance of generic forward protons, without overly affecting the signal efficiency. For a given Higgs mass, it is possible to calculate the expected distribution of momentum lost by the two protons. This can be easily translated into the $x-y$ distribution of the protons in the forward detector stations at 220 m. In particular, for the most difficult case of light Higgs masses, the lost momentum will be quite small; either both protons will be tagged in the detector stations at 420 m from the IP (which is impossible to trigger on, as discussed earlier), or one will be tagged at 420 m and one at 220 m. For the latter case, the $x-y$ distribution of protons from exclusive Higgs events ($m_H = 120$ GeV) in the detector station at 220 m is shown in Figure 2 (a). Signal protons are concentrated in the inner part of the detector i.e. within 4 mm of the detector edge. As we can see from Figure 2 (b), the background protons, which determine

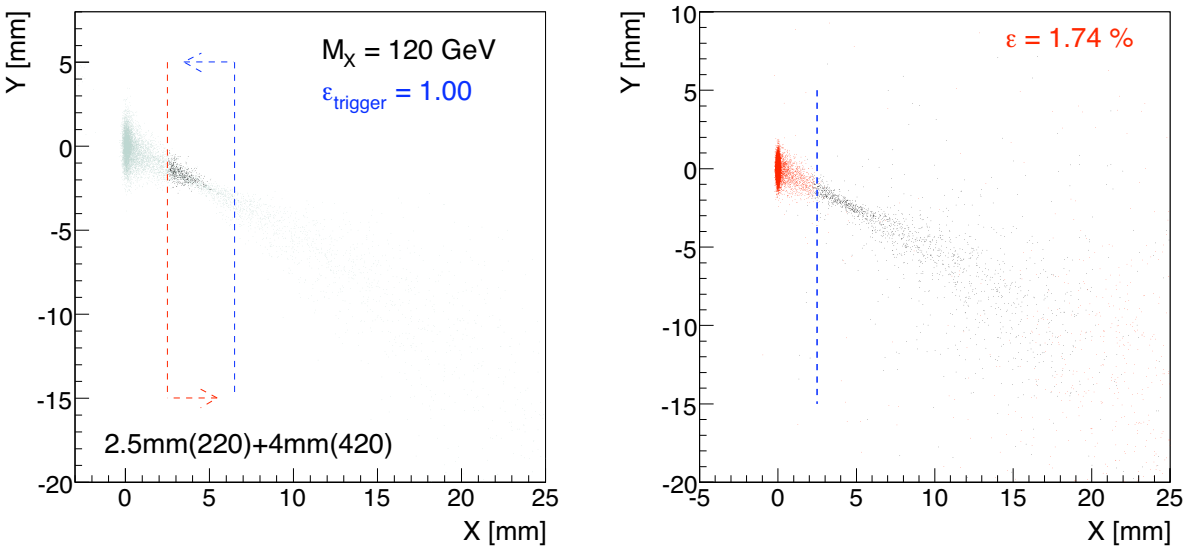

(a) (b)

Figure 2: The $x-y$ distribution of protons tagged in the detector stations at 220 m from the IP for exclusive Higgs mass of 120 GeV given that a proton is also present in a detector at 420 m on the other side (a). The corresponding plot for all events at the LHC is shown in (b). Protons are tracked through the LHC lattice using MAD-X [7] and cross-checked with FPTrack [8].

the L1 trigger rate, are spread over a larger distance. It has been calculated using events simulated by PYTHIA that the occupancy in the detector stations at 220 m drops by a factor of two simply by requiring that the protons lie within the 4 mm of the detector edge. The x distributions for different values of the Higgs mass are shown in Figure 3. It is clear that the majority of asymmetric events can be retained by triggering only on protons that are tagged on the inner side of the detector at 220 m.

In the subsequent sections, we assume that the detectors stations at 220 m will have an active detector edge 2.5 mm from the beam, and that the final design of the detector stations at 220 m will allow us to select events in which the proton is tagged in the innermost 4 mm of the detector. With these assumptions, the L1 rejection obtained by requiring a forward proton at 220 m ranges from approximately 14 at a luminosity of 2×10^{33} cm^{-2} s^{-1}, to 5 at 5×10^{33} cm^{-2} s^{-1} and about 3 at 10^{34} cm^{-2} s^{-1}.

4 Trigger efficiency for signal

Figures 4 (a) and 4 (b) show the jet trigger efficiency as a function of the leading jet's transverse energy for inclusive and exclusive dijet events respectively. The inclusive samples are fully simulated PYTHIA [9] di-jet events and the exclusive sample is fully simulated ExHuME [10] events (see Appendix A for details). The trigger items are 2J35 (jets are central, $|\eta| < 3.2$, with $E_T > 35$ GeV), J35+J23 (one jet with $E_T > 35$ GeV and the other with $E_T > 23$ GeV) and 2J42 (both with $E_T > 42$ GeV). Since in the process of writing this note, a proposal to round-off the thresholds has been made, we will also show some rates for a J40 + J20 configuration, to show that even this new trigger configuration will not change radically the results of this study.

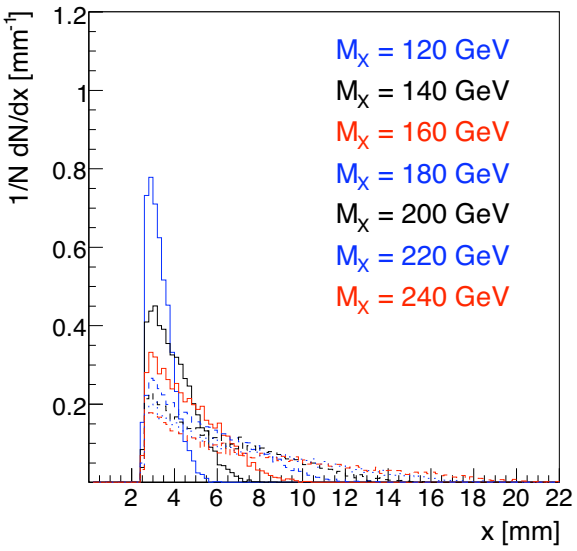

Figure 3: The x distribution of protons detected at 220 m from exclusive Higgs events of different mass, given that the other proton is tagged in the detector station at 420 m on the other side of the IP.

L1 item	Rate at 2×10^{33} (kHz)	Rate at 10^{34} (kHz)
J23	370	1850
J35	97	483
J42	52	259

Table 1: The expected single jet trigger rate at ATLAS.

We can see that the 'softest' di-jet threshold (J35+J23) is the only one that can give a reasonable efficiency for jets coming from light Higgs decays, with transverse energies of the order of 50-60 GeV. Keeping this result in mind, we now examine the rates of the three trigger configurations.

5 Expected rates for the various trigger configurations

We estimate the jet trigger rates using fully-simulated PYTHIA di-jet events and cross check the estimate using PYTHIA minimum bias (non-diffractive) events. A list of samples are given in Appendix A. Due to the lack of samples with pile-up, these numbers do not account for the added hadronic activity due to multiple proton-proton interactions in the same bunch-crossing. However, it can be expected that these numbers will not change too much after corrections to the trigger jet energy scale are applied for the average pileup deposit.

The available L1 bandwidth assigned to an AFP-based measurement of $H \to b\bar{b}$ will depend firstly on ATLAS discovery and then subsequently on the importance placed by the Collaboration on this channel - a reasonable estimate is about 2 kHz. Table 1 shows the rate of the single jet triggers and clearly these numbers would have to be heavily pre-scaled. Adding the requirement of a second jet (Table 2) does help - the J23+J35 trigger has a considerably smaller rate than the inclusive J35 trigger,

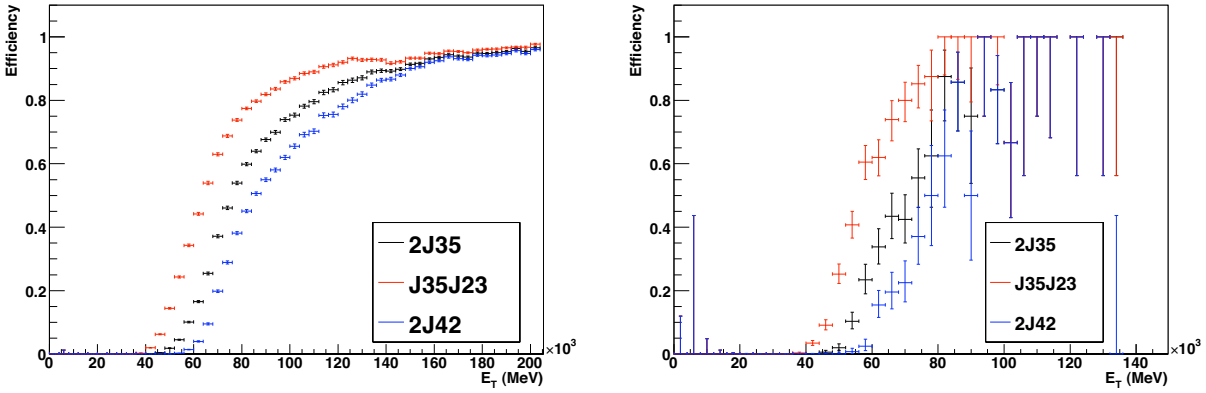

(a) (b)

Figure 4: The trigger efficiency for the J35+J23, 2J35 and 2J42 trigger items for (a) inclusive di-jet events and (b) exclusive events.

L1 item	Rate at 2×10^{33} (kHz)	Rate at 10^{34} (kHz)
2J23	84	418
2J35	24	118
J23+J35	52	261
2J42	14	68
J20+J40	43	216

Table 2: The expected di-jet trigger rate at ATLAS.

whilst the efficiency for signal events is comparable. However, we are still far from the estimate for the available rate.

Let us consider now the case in which at least one forward proton is detected in the AFP detector stations at 220 m in addition to the di-jets in the central calorimeter. As discussed in section 3, rather than considering the full AFP detector acceptance we assume that the trigger can select those protons in the inner 4 mm (i.e. the part of the detector that is closest to the beam position). The rates for the di-jet trigger plus forward proton requirement (p220) are shown in Table 3. We see that the addition of the forward proton tag reduces the rate by a factor of approximately 14 for a luminosity of 2×10^{33} cm^{-2} s^{-1}, but only by a factor of $\sim$3 at a luminosity of 10^{34} cm^{-2} s^{-1}. It should be noted that this is the best achievable rate given the present (not upgraded) ATLAS trigger configuration plus the addition of a L1 AFP trigger.

If the L1 calorimeter trigger is upgraded as discussed in section 2, additional handles can be utilized. The first possibility is to exploit the kinematic correlations between the pseudo-rapidities of the protons and the jets. This is especially useful as pile-up should not overly affect jet directions (unlike the jet energy) and so our results should be valid at the highest luminosities. Given the information from the 220 m detector stations, we know the side of the detector the candidate exclusive proton was tagged on. For a light Higgs ($\sim$120 GeV), the two jets from an exclusive event will be boosted in the direction of the proton tagged in the detector station at 220 m. We can therefore utilize the average di-jet rapidity,

$$\bar{\eta} = \frac{1}{2}(\eta_1 + \eta_2), \tag{7}$$

L1 item	Rate at 2×10^{33} (kHz)	Rate at 10^{34} (kHz)
2J23 + p220	6.0	144
2J35 + p220	1.7	41
J23+J35 + p220	3.7	90
2J42 + p220	1.0	23
J20+J40 + p220	3.1	75

Table 3: The rate for a di-jet plus forward proton trigger. The forward proton is required to be within the first 4 mm of the detector station at 220m from the IP.

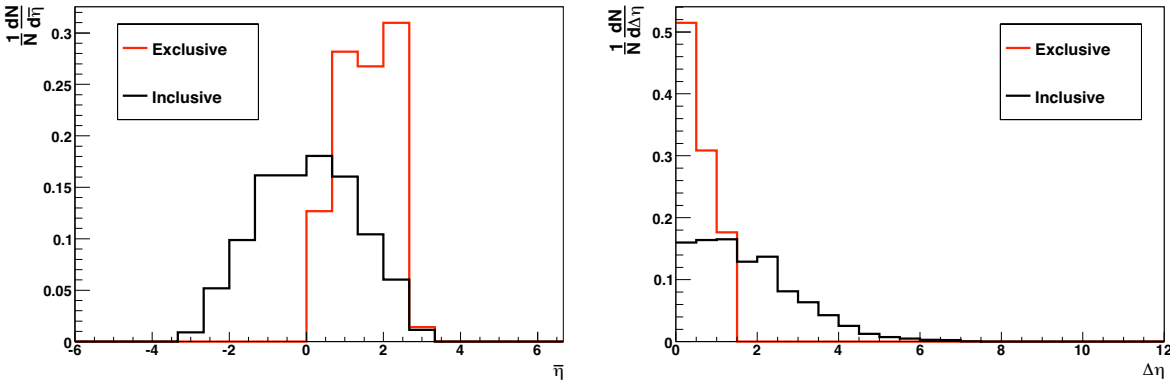

(a) (b)

Figure 5: The average di-jet rapidity given a proton tag in the detector station at 220 m on the A-side of the detector (a). The difference in pseudo-rapidity of the two leading jets (b).

where $\eta_{1,2}$ are the pseudo-rapidities of the two leading jets. Figure 5 (a) shows the average di-jet distribution for exclusive and inclusive di-jet events given that a proton is tagged on the A-side ($\eta > 0$) of the detector and that the J35+J23 threshold is passed. Note that the inclusive di-jet distribution is symmetric because the di-jet boost has no correlation with the proton tag. Thus we can utilize the L1 trigger requirement that

- $\bar{\eta} > X_A$ if the proton is tagged on the A-side of the detector and
- $\bar{\eta} < -X_A$ if the proton is tagged on the C-side of the detector,

where X_A is a threshold. The first two rows of Table 4 show the reduction in rate for the J23+J35 L1 di-jet trigger (plus forward proton), for values of $X_A = 0.5$ or $X_A = 1.0$. We choose the more conservative option, $X_A = 0.5$ in the remainder of the trigger discussion. At this point, the rate at a luminosity of 2×10^{33} cm^{-2} s^{-1} is around the 2kHz target, but the high luminosity rate remains far too large.

Another handle we can use is the requirement that jets coming from Higgs decays are relatively collinear. Figure 5 (b) shows the difference in pseudo-rapidity between the two jets, $\Delta\eta$, given by

$$\Delta\eta = |\eta_1 - \eta_2| \tag{8}$$

for signal and background events. The distributions are shown after all previous trigger requirements. The reduction in rate for $\Delta\eta < X_D$, where X_D is threshold of 1.5 or 2.0, is shown in the final three

L1 item	Rate at 2×10^{33} (kHz)	Rate at 10^{34} (kHz)
J23+J35 + p220 + X_A=0.5	1.4	34
J23+J35 + p220 + X_A=1.0	1.0	23
J23+J35 + p220 + X_A=0.5 + X_D=1.5	0.8	19
J23+J35 + p220 + X_A=0.5 + X_D=2.0	1.0	23
J20+J40 + p220 + X_A=0.5	1.1	28
J20+J40 + p220 + X_A=1.0	0.8	19
J20+J40 + p220 + X_A=0.5 + X_D=1.5	0.7	17
J20+J40 + p220 + X_A=0.5 + X_D=2.0	0.6	16

Table 4: The rates of the L1 trigger for J23+J35, plus forward proton, plus requirements on the pseudo-rapidity of the L1 leading jets.

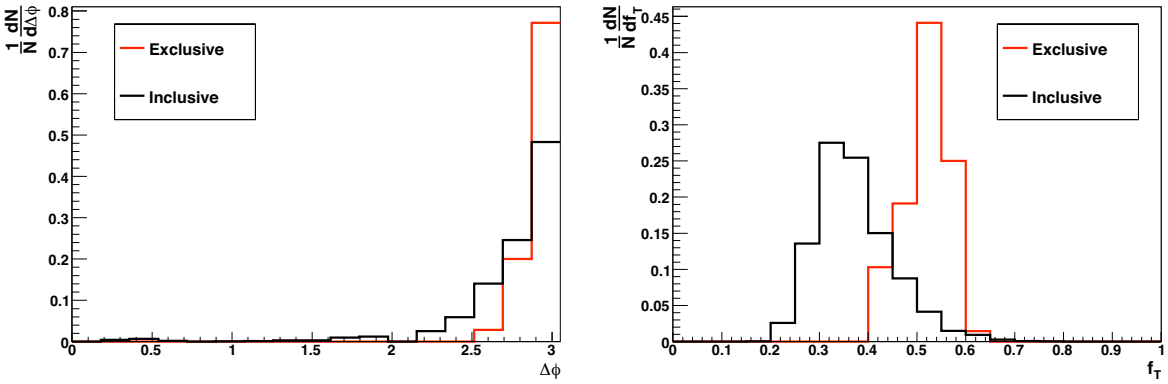

(a) (b)

Figure 6: The difference in azimuth of the two leading jets (a). The f_T distribution (b).

rows of Table 4. We see that an additional factor of almost 2 can be gained with this cut and it is encouraging that the L1 rate is now much closer to the goal of approximately 2kHz, although a largish pre-scale would be needed at the highest luminosity. We choose the requirement $X_D < 1.5$ in the final discussion that follows.

We can make further use of the exclusivity of the event. The lack of initial state radiation in central exclusive production means that the jets are relatively back-to-back in comparison to inclusive events. Figure 6 (a) shows the azimuthal separation of the leading jets. Secondly, the lack of underlying event activity in CEP events means that the majority of energy deposited in the calorimeter will be contained within the di-jet system. We define the transverse energy fraction, f_T, as

$$f_T = \frac{E_T^1 + E_T^2}{H_T} \tag{9}$$

where $E_T^{1,2}$ are the transverse energies of the two leading jets and H_T is the total transverse energy deposited in the calorimeters. Figure 6 (b) shows the f_T distributions for signal and background events. It should be noted that the effect of pile-up on this variable could be large and is unknown due to the lack of pile-up samples. Despite this, one may expect that some separation of signal and background using f_T will still be possible at high luminosities.

L1 item	Rate at 2×10^{33} (kHz)	Rate at 10^{34} (kHz)
J23+J35 + p220 + X_A=0.5 + X_D=1.5 + $\Delta\phi > 2.5$	0.61	14.8
J23+J35 + p220 + X_A=0.5 + X_D=1.5 + $f_T > 0.45$	0.12	2.9
J20+J40 + p220 + X_A=0.5 + X_D=1.5 + $\Delta\phi > 2.5$	0.51	12.2
J20+J40 + p220 + X_A=0.5 + X_D=1.5 + $f_T > 0.45$	0.12	2.9

Table 5: The final rate estimate for the exclusivity trigger given two different final trigger requirements, $\Delta\phi$ or f_T, as explained in the text.

L1 exclusivity	Signal efficiency (%)
X_A	92 ± 9
X_D	100 ± 12
$\Delta\phi$	99 ± 12
f_T	90 ± 13

Table 6: The signal efficiency for each L1 exclusivity requirement after the events have passed the di-jet trigger and the L1 proton tag (at 220 m) requirement. The low statistics of the signal sample is reflected by the relative errors, simply estimated as $1/\sqrt{N}$ where N is the number of events passing the cut.

Table 5 shows our final results. In the first scenario, we consider that the J35+J23 will be applied in conjunction with $X_A = 0.5$ and $X_D = 1.5$ and also that $\Delta\phi > 2.5$. In the second scenario, we consider that the J35+J23 will be applied in conjunction with $X_A = 0.5$ and $X_D = 1.5$ and also that $f_T > 0.45$. The first option is our conservative estimate as we assume that pile-up will render an f_T cut useless. The second option is our optimistic estimate, which assumes the f_T distribution will not be affected by pile-up. A realistic estimate is somewhere between the two extremes.

To put these results in context, the results published in [2, 3] assume that BSM Higgs scenarios, such as the MSSM and triplet Higgs models, can be observed with asymmetric tagging with a pre-scale of about 5. A prescale of 5 applied to the 'conservative' $\Delta\phi$ requirement would result in a trigger rate of approximately 2.5 to 3 kHz at 10^{34} cm^{-2} s^{-1}, which is not too much above the 2kHz target rate. If however, we assume that the f_T-based trigger is applicable at the highest luminosity, we would be able to achieve the 2 kHz target using a pre-scale of just 1.5.

The signal efficiency is shown in Table 6 for each of the calorimeter based L1 trigger requirements that are imposed after the initial di-jet trigger and proton acceptance. Given the low pre-scale, it seems reasonable that a L1 trigger can be constructed to retain exclusive $H \to b\bar{b}$ events with high efficiency by using forward proton detector and central calorimeter information.

5.1 Trigger rates without forward proton tagging at L1

So far, we have considered the case where a proton is tagged in the 220 detector, assuming that the other will be tagged in the 420 m one, even if this information is not available at trigger level. The acceptance of this asymmetric tagging decreases rapidly with the mass of the central system, and for the light Higgs case (120 GeV) more of the events have both protons tagged in the 420 m detectors; the acceptance for symmetric and asymmetric tagging is 20% and 17% respectively. It is therefore worth examining the trigger rates if no forward proton information is used in the L1 trigger decision, to see if the obvious loss of performance due to the lack of proton tagging can be compensated by the

L1 item	Rate at 2×10^{33} (kHz)	Rate at 10^{34} (kHz)
J23+J35 + X_D=1.5 + $\Delta\phi > 2.5$	22	111
J23+J35 + X_D=1.5 + $f_T > 0.45$	4.2	21
J20+J40 + X_D=1.5 + $\Delta\phi > 2.5$	18	92
J20+J40 + X_D=1.5 + $f_T > 0.45$	4.2	21

Table 7: The final rate estimate for the exclusivity trigger with no forward proton information, given two different final trigger requirements, $\Delta\phi$ or f_T, as explained in the text.

higher acceptance for low-mass Higgs production.

In the case of no proton tagged at 220 m, not only do we lose the rejection factor of 14 (3) at 2×10^{33} cm^{-2} s^{-1} (10^{34} cm^{-2} s^{-1}) from requiring that a proton is tagged in one of the detector stations, but we also lose the rejection provided by correlating the average di-jet rapidity with the proton tag. Table 7 shows the final results assuming no proton information at L1; $\Delta\phi$ is again used as the conservative estimate and f_T as the optimistic estimate.

The final rates at high luminosity are approximately seven times larger than the rates obtained using forward proton information, implying that the subsequent prescale would have to be seven times larger and the (overall) signal efficiency seven times smaller. However, for a light Higgs mass, the situation is somewhat improved because the *non-proton* trigger strategy will also retain symmetric events (i.e. those events with both protons tagged at 420 m). Given the baseline active edges of the AFP detectors, the acceptance for a 120 GeV Higgs boson is 28% and 17% for symmetric/asymmetric events respectively. However, as the mass increases, the acceptance for symmetrically tagged events decreases, whereas the acceptance for asymmetrically tagged events increases. Therefore, the (overall) effect of removing the proton information at L1 is a factor of 2.5 loss in efficiency for a Higgs mass of 120 GeV and a much larger loss at higher Higgs masses.

6 Conclusions

The $H \to b\bar{b}$ channel is one of the most challenging for the proposed AFP upgrade, due to the low signal cross section and large background. Successful measurements will depend on the implementation of an efficient trigger with low pre-scale. As expected, a di-jet trigger based only on central detectors is not sufficient to keep a reasonably low L1 rate without big prescales, so information from the AFP detector stations will be required in addition to an upgrade of the L1 calorimeter trigger. In particular the following information must be available:

- The forward proton trigger must be able to trigger only on protons that hit the inner 4 mm of the detector station at 220 m. This means that the sensitive triggering area has to be smaller than the active detector, or that some form of segmentation has to be present.

- The L1 calorimeter must be capable of defining new exclusivity criteria, outlined in section 5, using the E_T, η, and ϕ of the two leading jets.

Using those two ideas, it is possible to keep rates down for thresholds that still provide a reasonable efficiency for low-mass Higgs detection. This should be true even up to the highest luminosities for the exclusivity conditions based on angular information. Extremely good, additional, rejection was observed for the exclusivity criterion, f_T, which utilizes the ratio between jet transverse energies

and the total scalar sum of transverse energy in the detector. However, further work with (currently unavailable) pile-up samples is necessary to determine the effect of pile-up on the f_T variable at the highest luminosities.

Acknowledgments

We would like to thank Andrew Brandt, Norman Gee and Thorsten Wengler for useful discussions and comments throughout this work.

A Monte Carlo event samples

The PYTHIA di-jet samples used in the analysis were:

`mc08.005010.J1_pythia_jetjet.recon.AOD.e323_s400_d99_r474`
`mc08.005011.J2_pythia_jetjet.recon.AOD.e323_s400_d99_r474`
`mc08.005012.J3_pythia_jetjet.recon.AOD.e323_s400_d99_r474`
`mc08.005013.J4_pythia_jetjet.recon.AOD.e323_s400_d99_r474`
`mc08.005014.J5_pythia_jetjet.recon.AOD.e323_s400_d99_r474`
`mc08.005015.J6_pythia_jetjet.recon.AOD.e323_s400_d99_r474`
`mc08.005016.J7_pythia_jetjet.recon.AOD.e323_s400_d99_r474`
`mc08.005017.J8_pythia_jetjet.recon.AOD.e323_s400_d99_r474`

Note that *JX* denotes the parton p_T range of each sample i.e. J1 refers to $17 < p_T < 35$ GeV. Thus the samples can be summed together to give good efficiency for a large range of jet transverse energy. The rates were cross-checked with the PYTHIA minimum bias sample:

`mc08.005001.pythia_minbias.recon.AOD.e306_s400_d99_r474`

The exclusive sample, used to determine the cut values and efficiencies, was

`mc08.106065.ExhumeGG_Et35.merge.AOD.e386_s495_r635_t53`

which is a 10TeV *gg* sample. However, we expect the results to not be much different for 14TeV Higgs sample because we restricted the central mass to be in the range $110 < M < 140$ GeV. Thus the topology of the di-jets should be approximately correct.

References

[1] V. A. Khoze, A. D. Martin and M. G. Ryskin, "Prospects for new physics observations in diffractive processes at the LHC Eur. Phys. J. C **23**, 311 (2002) [arXiv:hep-ph/0111078].

[2] M. G. Albrow and A. Rostovtsev, arXiv:hep-ph/0009336. J. R. Ellis, J. S. Lee and A. Pilaftsis, Phys. Rev. D **71**, 075007 (2005) B. E. Cox, F. K. Loebinger and A. D. Pilkington, JHEP **0710** (2007) 090 S. Heinemeyer, V. A. Khoze, M. G. Ryskin, W. J. Stirling, M. Tasevsky and

G. Weiglein, Eur. Phys. J. C **53** (2008) 231 J. R. Forshaw, J. F. Gunion, L. Hodgkinson, A. Papaefstathiou and A. D. Pilkington, JHEP **0804** (2008) 090 M. Chaichian, P. Hoyer, K. Huitu, V. A. Khoze and A. D. Pilkington, arXiv:0901.3746 [hep-ph].

[3] The FP420 R&D Project: Higgs and New Physics with forward protons at the LHC. By FP420 R and D Collaboration (M.G. Albrow et al.). FERMILAB-FN-0825-E, Jun 2008. 176pp. e-Print: arXiv:0806.0302 [hep-ex]

[4] Norman Gee private communication.
See also (for instance) N.Gee's talk at the latest Rome TDAQ week: http://indico.cern.ch/materialDisplay.py?contribId=23&sessionId=4&materialId=slides&confId=56544

[5] ATLAS forward detectors for Measurement of Elastic Scattering and Luminosity Determination: Technical Design Report ATLAS-TDR-018 ; CERN-LHCC-2008-004.

[6] A. Brandt, S. Kolya and J.Pinfold, in preparation.

[7] F. Schmidt, P. K. Skowronski and E. Forest, *In the Proceedings of Particle Accelerator Conference (PAC 07), Albuquerque, New Mexico, 25-29 Jun 2007, pp 3381.*
H. Grote and F. Schmidt, *In the Proceedings of Particle Accelerator Conference (PAC 03), Portland, Oregon, 12-16 May 2003, pp 3497.*

[8] P.Bussey, private communication

[9] PYTHIA 6.400 manual, published in JHEP 05 (2006) 026 (LU TP 06-13, FERMILAB-PUB-06-052-CD-T, hep-ph/0603175)

[10] J.Monk, A.Pilkington Comput.Phys.Commun.175:232-239,2006.

Conceptual Design of a New 220 m Trigger Detector

Andrew Brandt (UT-Arlington), Scott Kolya (Manchester), Jim Pinfold (Alberta)

Introduction

In order to gain maximal benefit from the 220 m AFP detectors it is critical to have L1 trigger capabilities. This is a necessary requirement for triggering on light Higgs in the case where one of the protons is in a 220 m detector, and the other is in a 420 m detector on the opposite side [Physics note], and would be useful for many other physics topics. The key issues are developing a highly efficient flexibly segmentable trigger detector that can operate within the ATLAS L1 trigger latency.

The Detector

A conceptual design for a Quartz-fibre based trigger detector (QFT) utilizing Cerenkov light and a microchannel plate photomultiplier tube (McPMT) is presented in Fig. 1. In this scheme there are two identical detector units (shown with a small separation in the z direction for ease of understanding, although they may be contiguous or else one could be located at z=216 m and one at 224 m) each comprised of a rectangular bundle of thin clad fused-silica (or quartz) fibres. The bundle has a cross-sectional area of 24mm (x) x 12 mm (z) and overall length of about 10 cm (y). The first 6 cm of the bundle, in the y direction, is formed into a solid matrix (potted), while the last 4 cm of the fibre bundle are left free in order that the fibres corresponding to various trigger regions can be mapped onto distinct regions of the McPMT.

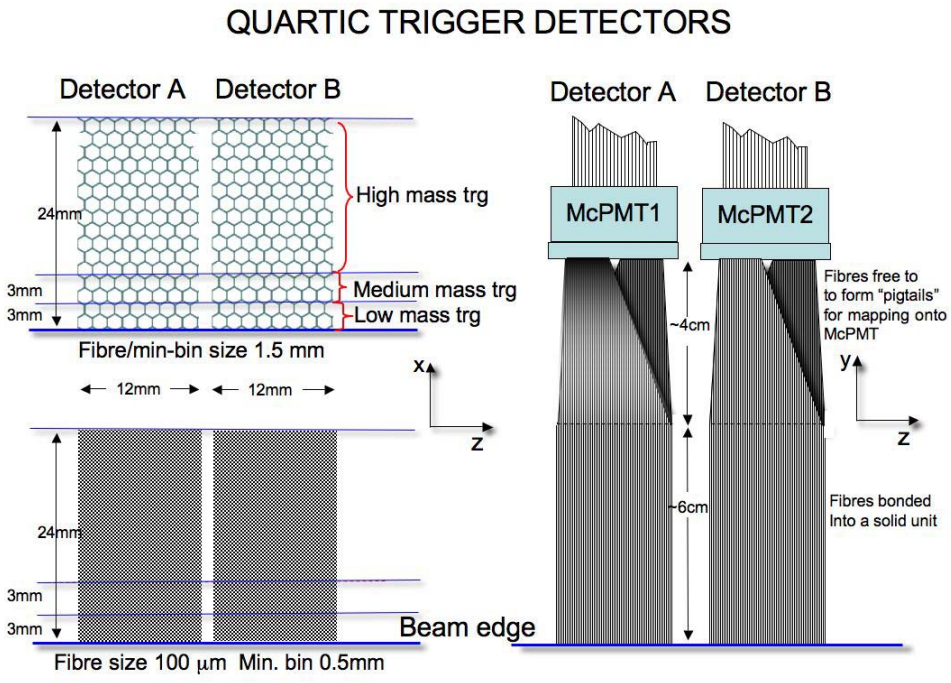

Figure 1: Conceptual design of QFT, a quartz fiber-based L1 trigger detector, as described in text.

The corresponding, adjacent, regions of the two detectors (A & B) are placed in coincidence, in order to minimize noise triggers. Two fibre sizes are considered: 100 micron diameter, to ensure fine edge definition and spatial resolution; and 1.5 mm diameter, which has the advantage of ease of manufacture. One could also have a composite bundle with small diameter fibres near to the beam edge and larger fibres further from the beam edge. GEANT-4 based simulations will be done to investigate the three options, and a pre-prototype will be tested in fall 2009 in test beam.

The segmentation could be as small as 0.5 mm for the smaller fiber diameter, and will be optimized based on further physics and detector simulations and testing.

From experience with the LUCID detector, and taking into account McPMT quantum efficiency and attenuation in the fibres, we estimate that a proton traversing the 12mm deep (in *z*) fused silica bundle of each detector element of the QFT would result in the order of 50 PEs captured in the McPMT. This signal level is entirely adequate to obtain the optimum response from the proposed trigger electronics discussed below.

Trigger Readout

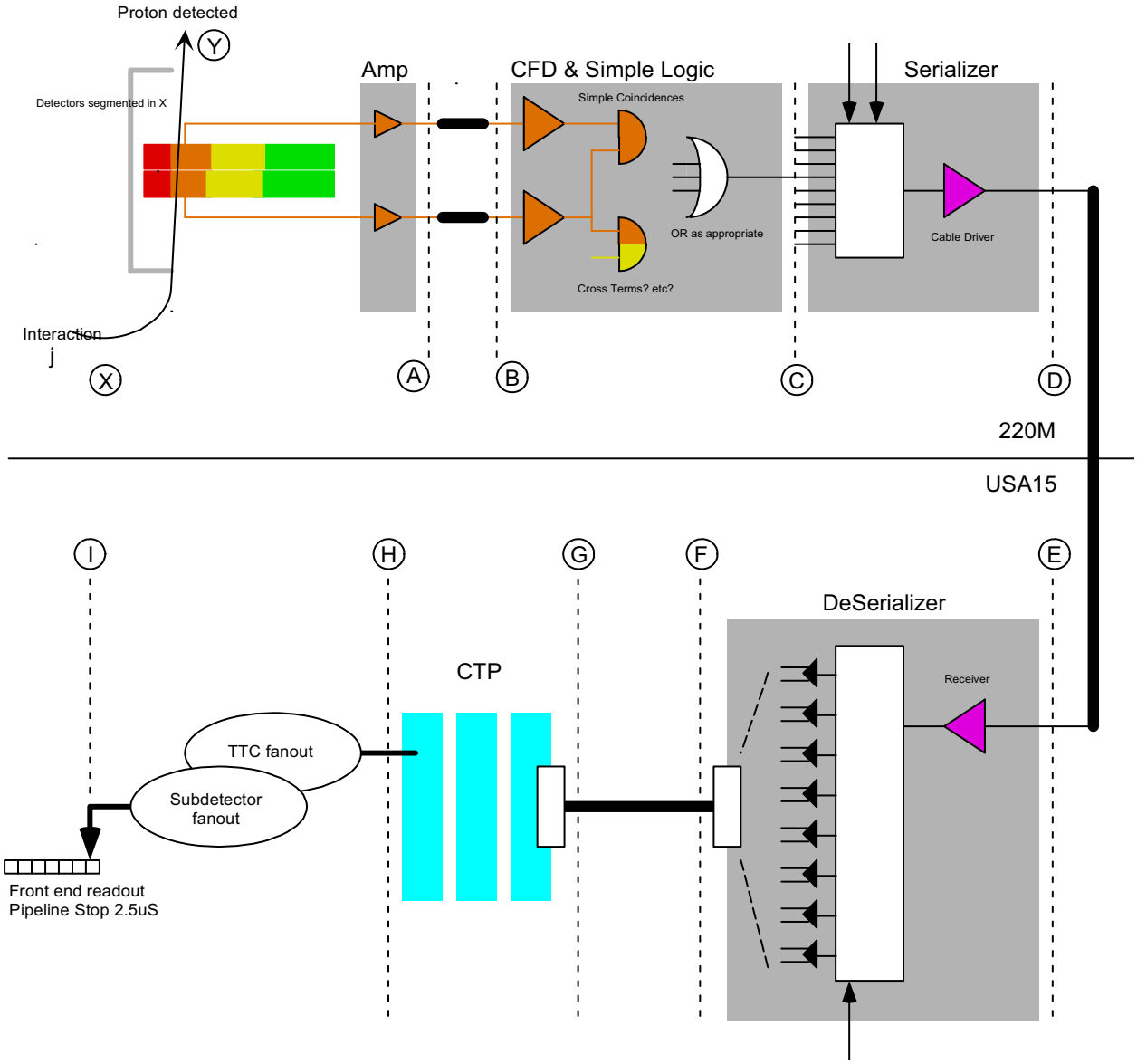

Figure 2: Conceptual design of the QFT readout electronics QFT, as described in text.

Figure 2 shows the layout of the readout. Radiation tolerant amplifiers are placed near the detector and drive signals to the trigger logic which is positioned as near as possible in a less active area (e.g. under magnets or in the nearby alcove).The signals are discriminated and simple combinations formed to give a number of bits corresponding to the segmentation of the detector.

Cross elements could be formed, but the compact nature of the detector and very small angular divergence of the beam makes these unnecessary.

The total number of trigger bits we send back to ATLAS for L1 is a balance between optimal binning to give the lowest background trigger rate (when combined with the calorimeter) and the practical limits on the number of cable connections we can make, serial transmission schemes, and CTP input availability.

The simplest scheme involves sending one or perhaps as many as four bits directly over individual cables (low, intermediate, high mass, and any coincidence, for example). Large diameter air core cables are required to minimize the cable delay, so it is impractical to lay more than four per side. This scheme has the advantage that is has the lowest possible latency, as it avoids serialization overheads.

The alternative is to send a serial stream of bits over a single cable. Over distances of 250 m we can comfortably send data at rates around one Gbits/sec over a direct link without repeaters. We need to use 40Mhz, or a multiple, as our reference clock, so our baseline plan is to transmit data at 800Mbits/s, which, allowing for 8B/10B encoding, corresponds to a 16 bit word size at a 40 Mhz rate. A bit rate of 1.6Gbits/sec may also be possible with more sophisticated pre-emphasis and equalization, this would not only increase the number of bits that could be sent in each machine clock tick, but also would substantially reduce the latency of the serialization. The output of the receiver in USA15 will drive signals to the CTP_IN board directly by LVDS or indirectly by NIM levels.

Latency Estimate

The ATLAS L1 central trigger processor (CTP) receives trigger bits, processes them to form the final L1 decision, and distributes them through the TTC system to the sub-detectors. The front end buffers of ATLAS sub-detectors have been designed to a specification that requires this trigger to be received no later than 2.5 μs, which leads to a hard requirement that the trigger bits arrive at the CTP no later than 2.0 μs after the interaction. Allowing for a safety margin this leads to a specification of no later than 1.9μs with a suggested target of 1.8 μs or better.

The ‘worst case scenario’ delays from the various parts of the system and the resulting overall latency at each point are given in the tables below. Some estimates are based on the corresponding solution in place for Alfa [TDR], summarized here:

Item		**Time (ns)**
Particle path from IP to RP	240(m) x 3.3357 (ns/m)	800
Signal treatment in local electronics	Shaper peaking time and driver	40
Signal transmission from RP to CTP	295 (m) x 3.666 (91% c) (ns/m)	1081
Signal treatment in USA15	Discrimination	20
Total		**1941**

Table 1: ALFA Latency.

In particular, the most important input to the overall timing calculation is the route and resulting length of the long cable from the detector region back to the main ATLAS electronics. We assume that the route used by ALFA is optimal and we have used the same cable length, adjusted only by the position of our detectors (the ALFA cable route follows the LHC tunnel at least as far as the 220 m position). In the worst case one or both detectors are located at 224 m giving us an overall cable length of 279 m, compare to the 295 m ALFA cable. As for ALFA, our timing calculations are based on using low density foam dielectric cable (air-core) with a relative propagation speed of 91%. Note that the ALFA cable path runs directly to the area of the ATLAS CTP rack.

The local electronics will be positioned as close to the optimal route as possible: we have estimated an additional 'detour' delay here as the exact positioning is yet to be determined. Our existing prototype CFDs show pulse to pulse timing jitter of much better than 1 nsec and the simple combinatorial logic can be implemented in discrete logic or a fast CPLD with a low latency. The serialization and de-serialization would be performed by dedicated commercial parts. The latencies have been calculated using the manufacturer's worst case specification.

Delay	**Description**	**Time (ns)**
X- Y	Time of flight of Proton to detector at 224m	750
Y-A	Proton strike to amplifier output.	10
A-B	Extra cable delay introduced by positioning of the semi-local electronics (worst case, in alcove)	30
B-C	CFD (latest output) and logic	15
C-D	Direct cable connection (no serializer)	5
C-D	Serializer latency (strobe to 1st bit) 800Mb/s	55
C-D	Serializer latency (strobe to 1st bit) 1.6Gb/s	35
D-E	Long cable to USA15 from electronics (279)	1025
E-F	Direct cable connection	12
E-F	De-Serializer latency (1st bit to output) 800Mb/s	150
E-F	De-Serializer latency (1st bit to output) 1.6Gb/s	85
F-G	Time to CPT_IN connector	10

Table 2: The various components of the trigger latency; different options for the timing for C-D and E-F depending on the exact data transfer scheme.

	Y	**A**	**B**	**C**	**D**	**E**	**F**	**G**
	Particle hits Detector	Output from Amplifier	Input to CFD & Logic	Input to Serilaizer	Output to Cable (1st bit)	In from Cable (1st bit)	Output from DeSerializer (strobed)	Input to CTP_IN
Dedicated Cable(s)	750	760	790	805	810	1830	1842	1852
Serial bits 800Mb/s	750	760	790	805	860	1885	2035	2045
Serial bits 1.6Gb/s	750	760	790	805	840	1865	1950	1960
Alfa TDR (Comparison)	800	840				1921		1941

Table 3: A comparison of the latency of total latency of the different options.

Clearly, the dedicated cable scenario with at most a few trigger lines is close to the target and could be incorporated into ATLAS without further work, providing an immediate trigger option

available for the initial installation at 220 m, as early as 2011, and is the baseline design assume in the L1 trigger note. This maps well to the limited availability of spare trigger input bits for the existing ATLAS trigger implementation. Our trigger would be configurable in the combinatorial logic local to the detector, for example we could select a global 'any proton' trigger, a narrow energy band based on just one segment of the detector, or anywhere in-between.

The serial data stream options get very close to the specification, despite being worst case calculations. This approach may become useful part of the overall 'Phase 1' upgrade of the trigger system, where combining our energy bins with the enhanced calorimeter information would allow a very well targeted trigger for some classes of events, such as a light Higgs.There is definitely scope to improve these timings, for example, placing a trigger detector at 216 m rather than 224 m saves 30 ns in time of flight and almost 35 ns in cable delays.

Conclusion

We have presented the conceptual design of a flexible Level 1 trigger and readout system capable of providing a simple trigger from the 220 m proton detectors within the required ATLAS latency period. The detector and readout are both based on known technology, and the system would be straight-forward and inexpensive to design, build, and test. There are interesting opportunities for this to evolve to give more sophisticated, narrowly targeted triggers as part of the Phase 1 upgrade.

Plans to Address Phototube Lifetime Issue for AFP Fast Timing Detectors

Andrew Brandt (UT-Arlington) for AFP timing group

June 25, 2009

1. Introduction

The high expected rates of diffractive protons in the acceptance of timing detectors at 420 m and 220 m are a potential concern for the microchannel plate photomultiplier tubes (MCP-PMT) that are an essential component of these detectors. Figure 1(a) and (b) show one of the baseline timing detectors QUARTIC, a quartz (fused silica) based Cerenkov detector, which consists of an array of 4 x 8 6 mm x 6 mm bars quartz bars mapped to similar sized pixels of an MCP-PMT. A single proton passes through 8 consecutive bars, resulting in eight independent measurements of the proton time, allowing a precise measurement of the proton time O(10 ps). QUARTIC was initially conceived by Mike Albrow (Fermilab), and has been developed by Jim Pinfold (Alberta), Mike and me. Figure 1(c) shows GASTOF, a single-channel gas-based Cerenkov detector (developed by Krzysztof Piotrzkowksi of Louvain).

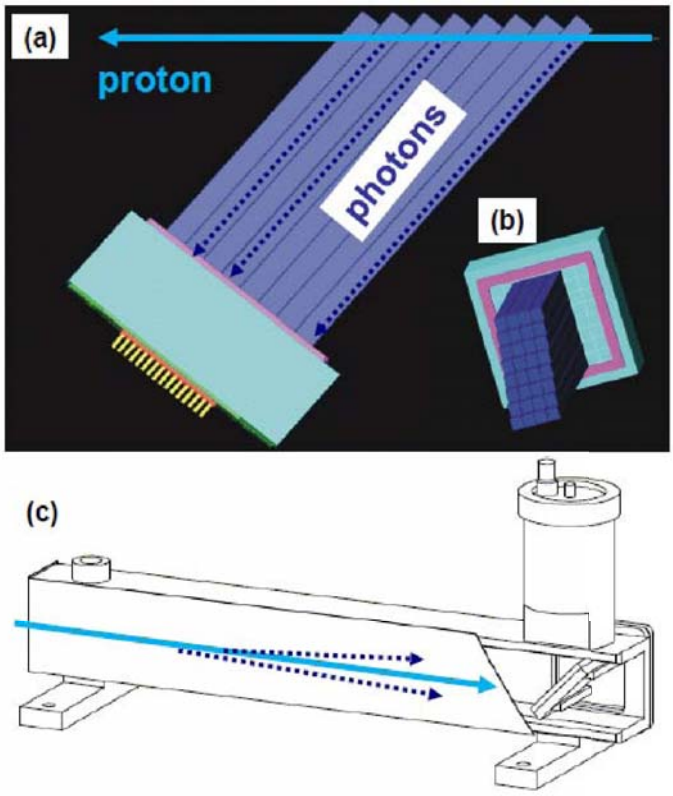

Figure 1: The baseline timing detectors: (a), (b) show the 4 x 8 quartz bar QUARTIC and (c) the GASTOF Cerenkov detectors.

From PHOJET simulations about 1% (3%) of interactions are expected to have a proton in our acceptance at 420 (220) m. With an expected average number of interactions ranging from about 5 to 25 over the luminosity range of $2x10^{33}$ $cm^{-2}s^{-1}$ to 10^{34} $cm^{-2}s^{-1}$ for 25 ns bunch spacing (40 MHz interaction rate), this implies proton rates ranging from 2 (6) MHz at 420 (220) m at $2x10^{33}$ luminosity to up to 10 (30) MHz at 220m at 10^{34} (PYTHIA predicts similar rates at 420 m, and about 20-30% lower rates at 220 m depending on the exact detector positioning with respect to the beam). In the current QUARTIC design, the hottest 6 mm x 6 mm pixel of a multi-anode MCP-PMT would see about half that rate, while an un-segmented GASTOF would see the full rate, but over a 3 times larger area (a single anode MCP-PMT with an area of 1 cm^2 is used in the baseline GASTOF design). Thus the MCP-PMT's should be able to cope with absolute rates of 15 to 30 MHz, or up to about 50 MHz/cm^2 at 10^{34} $cm^{-2}s^{-1}$. Primarily this note will focus on the QUARTIC MCP-PMT's (see Fig. 2), with some comments on the GASTOF design at the end.

These large proton rates are a concern for two main reasons : i) instantaneous current limitations of the tube required to sustain the high rates ii) lifetime of the tube from the effects on the tube of these rates integrated over time.

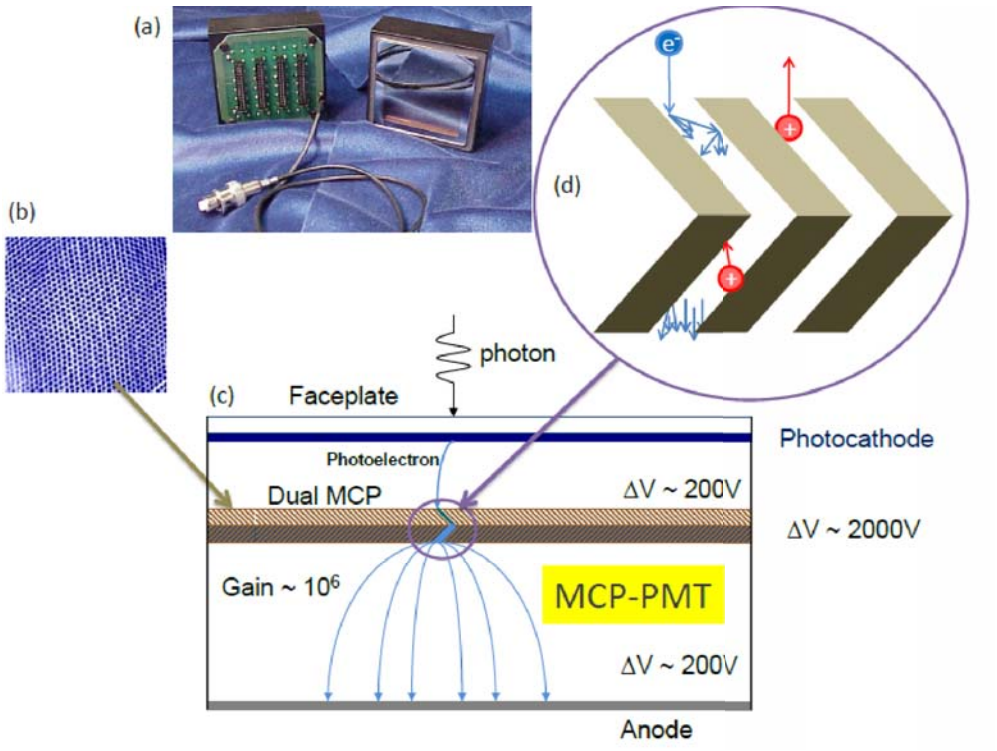

Figure 2: (a) photograph of a Burle 85011-501 64 channel MCP-PMT (b) photograph of an MCP (c) cartoon of the operation of an MCP-PMT (d) insert showing charge multiplication in pore and emission of positive ions that degrade the photocathode.

2. Rates and Currents

After receiving a photoelectron, a given pore of the PMT requires on the order of a millisecond to fully recover, so at high rates there is gain saturation, as enough pores are "busy" that the gain is effectively reduced. This rate limit is really a limitation in the amount of instantaneous current that can be extracted: if the anode current required to operate at a certain rate exceeds the current limit of the tube, the tube will still operate, but at reduced gain. The expression for anode current (I) is given below:

Anode Current = particle rate x number of photoelectrons per particle x electron charge x gain

Equation 1: $$I = R \bullet N_{pe} \bullet e \bullet G$$

For 10 pe's, a typical value for these detectors, and an electron charge of 1.6 x 10^{-19} C, the required anode current can be expressed as 1.6 μA/MHz for 10^6 gain, 0.16 μA/MHz for 10^5 gain, etc. For a 15 MHz proton rate in a 0.36 cm^2 at 10^6 gain, this would require about 70 μA/cm^2!

A rule of thumb is that one can extract about 10% of the strip current, where the strip current is the voltage of the tube divided by the resistance of the MCP glass. Tube limitations are often quoted in terms of the maximum average anode current, but the relevant quantity is really current per unit area as the current limit is a local limit (it does not improve the limit to use a small portion of a big tube). For a standard 25 μm pore Burle Planacon tube (Burle is a subsidiary of Photonis [1]), the maximum anode current is listed as 3 μA (corresponding to a 30 μA strip current), which for the 5 cm x 5 cm Planacon corresponds to a limit of about 0.1 μA/cm^2 . Newer versions of the Planacon have been made with a 10 times higher current limitation, and the absolute limit is expected to be no more than 2 to 3 times this, due to heating of the MCP's and other concerns. It should be noted that these limits apply to 25 μm pore tubes, and that the situation can be improved by going to smaller pore sizes, which increases the number of pores per unit area, effectively allowing a larger current to be extracted than the 10% "rule".

Given an absolute limit of a few μA/cm^2 and a maximum anticipated current of 70 μA/ cm^2 for the most populated pixel assuming a 10^6 gain, the only choices are to either i) abandon MCP technology or ii) to substantially reduce some combination of the number of pe's, the gain, or the proton rate. We have been studying the latter option and present results below. To summarize, the rate issue with standard tubes is a factor of several hundred, but technology is in-hand (smaller pore size, higher current MCP's) that reduces this discrepancy factor between the current required and the current obtainable to less than 20. We demonstrate below that this factor of 20 can be obtained by operating the tube at a gain of 5 x10^4 instead of 10^6.

3. MCP-PMT Lifetime

A closely related issue is the expected lifetime of the phototube. The leading cause of damage to the MCP-PMT's is damage to the photocathode from back-scattered positive ions, causing a decrease in quantum efficiency. The damage is generally believed to be proportional to the total extracted charge, which is the anode current integrated current over time ($Q=I\Delta t$). For a canonical LHC year of 10^7 seconds, a 70 $\mu A/cm^2$ anode current would correspond to 700 C/cm^2, whereas the limitation on existing tubes is believed to be on the order of 1 C/cm^2, with the lifetime defined as the point at which the gain is reduced by a factor of two. Figure 3 shows a lifetime measurement of the Hamamatsu R3809U-50 series MCP-PMT, the type of PMT used for GASTOF prototype tests. The 50% gain loss point is close to 1C for this 1 cm^2 active area tube, although results may vary depending on the exact photocathode used, wavelength considered, and details of the tests (not available). For the Burle tube, an integrated charge of 10 to 13 Coulombs over the 25 cm^2 area of the tube resulted in a 50% reduction in quantum efficiency, implying a lifetime of about 0.5 C/ cm^2 [2], although the exact details of the test, wavelength etc., are not available. One can conclude, based on this limited data, that a worst case value for the initial discrepancy factor between the required lifetime (700 C/cm^2) and the expected lifetime (0.7 C/cm^2) is about a factor of 1000 given a gain of 10^6. Increasing the current capability of the tube, which helps solve the rate issue, does not address the lifetime issue. Consequently, the only immediate factor that can be applied to reduce this 1000 discrepancy is a reduction of the gain by a factor of 20, which would reduce the integrated charge received by the tube to 35 C/cm^2, still a factor of about 50 too high for existing tubes.

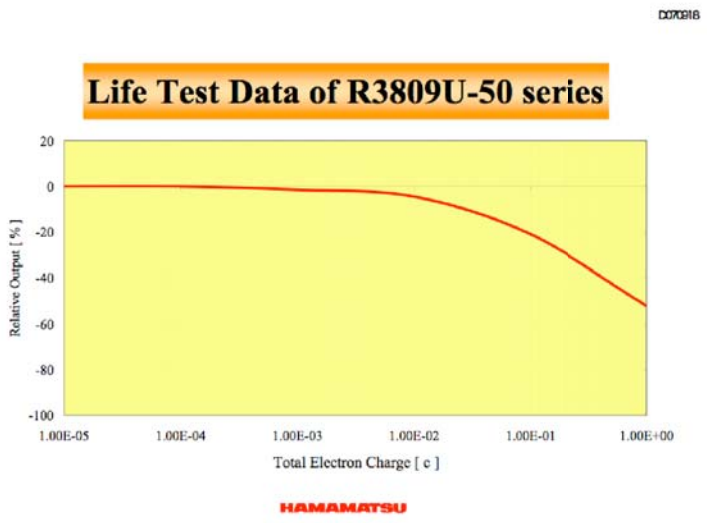

Figure 3: Lifetime measurements of the Hamamatsu R3809U MCP-PMT indicate a lifetime of about 1 C/cm^2.

The limited lifetime is a well-known issue faced by any experiment that desires to use MCP-PMT's in a high rate environment. This includes proposed high luminosity "Super B factories" in Italy [3] and Japan [4], for rare decay searches, and detailed studies of CP violation; the PANDA experiment [5], a high precision high luminosity fixed target experiment using a cooled antiproton beam to perform charmonium spectroscopy and search for glueballs and exotic states; and the NA62 Kaon experiment [6]. Significant work has been done to address this concern. One of the proven approaches is the application of an ion barrier, a thin metal layer placed on top of the MCP to suppress positive ion feedback. This was originally developed by the military for Gen III night vision tubes [7], and was observed to increase the tube lifetime by about a factor of 5 with gallium arsenide photocathodes. The reason that this has not been adopted as a standard feature of MCP-PMT's is that the barrier also has an undesirable side effect of partially blocking photoelectrons, resulting in a 40% reduction in collection efficiency.

Nagoya [8] has been a leading group in detector development using MCP-PMT's and their recent lifetime measurements [9] are especially relevant for us. In Fig. 4, they compare standard tubes with no aluminum barrier to specially made tubes with an ion barrier and observe a significant decrease in the degradation rate of the quantum efficiency at 400 nm for the Hamamatsu tube with the barrier compared to the standard one. They estimate a factor of 5-6 improvement in lifetime of their multi-alkali photocathode tube, based on this result and their measurement of the reduction in late pulses characteristic of positive ion back-scattering. They also tested tubes from the Budker Institute of Nuclear Physics (BINP) with and without the ion barrier and got mixed results (other curves in Fig. 4), which are plausibly explained by a less effective application of the ion barrier as evidenced by very little change in the collection efficiency between tubes with and without the barrier, combined with the smaller bias angle of the microchannels (5° on the BINP tubes compared to 13° for the Hamamatsu tubes), which is less effective at restricting the positive ion feedback.

Another very important related result from Ref. [9] is the wavelength dependence of the damage. Figure 5 shows that the damage to the photocathode, as evidenced by the ratio the QE before and after irradiation, is negligible for small wavelengths and dramatically more severe for large wavelengths. Given the $1/\lambda^2$ dependence of Cerenkov radiation, measuring the damage at 400 nm is an overestimate of the integrated QE loss, and in fact they measured only a 13% reduction in the number of accepted photons with their detector using the aluminum barrier Hamamatsu tube before and after irradiation.

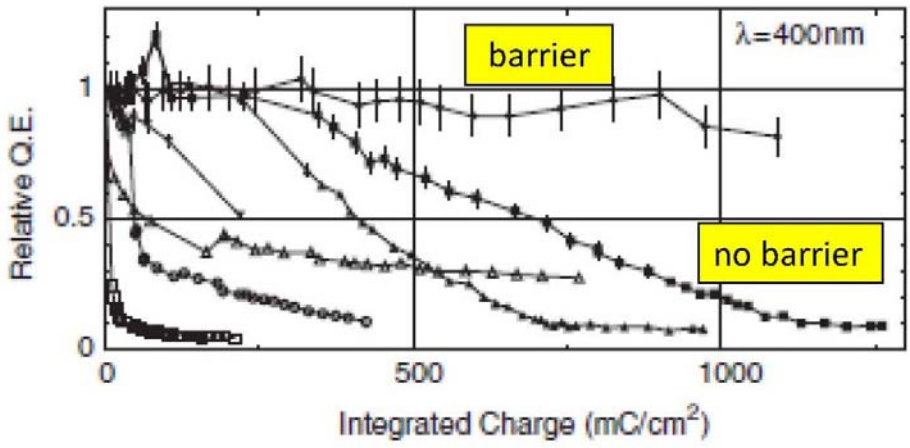

Figure 4: Relative quantum efficiency as a function of integrated charge for MCP-PMT's with and without an ion barrier [9].

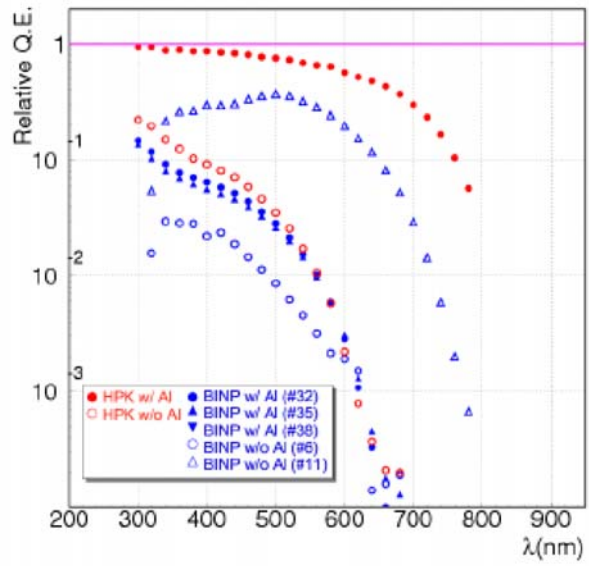

Figure 5: Relative quantum efficiency as a function of wavelength [5] for tubes with and without an ion barrier.

Another approach to reducing the positive ion feedback, adding a third MCP, has recently been tested by the BINP group [10]. The third MCP (combined with the other two forms a so-called Z stack) creates an additional barrier for ions, most of which appear near the anode (where the density of electrons in the avalanche is maximum), and are thus unable to navigate their way back to the cathode. This approach does not protect the cathode from ions produced in the first two MCP's, but these are less prevalent in the three stage design, since the extra gain provided by the third MCP allows a reduced voltage across the first two MCP's, reducing positive ion production. They infer a factor of 10 lifetime

improvement using this approach based on a reduction of the quantum efficiency at high wavelengths. Since the QE degrades quickly at high wavelength, accelerated lifetime tests are less time consuming, once the relationship between aging and wavelength has been measured.

Drawing on these and other ideas discussed below, we present a program to produce a longer lifetime PMT capable of surviving these high levels of integrated charge. First, we note that another possible lifetime issue is damage to the microchannel plates themselves, which would cause a reduction in the gain of the tube. Discussions with the Photonis, USA MCP division indicates that this is not an issue for our expected charge levels using their extended duration MCP glass, as shown in Fig. 6 [7].

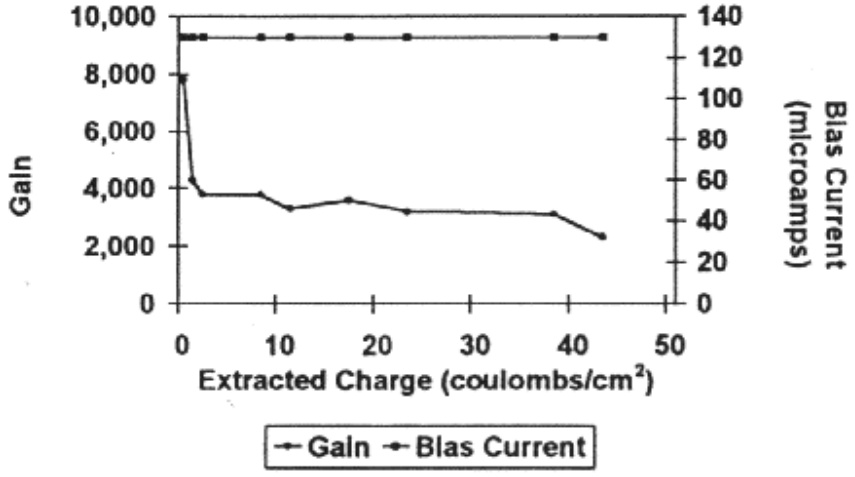

Figure 6: The typical gain degradation of a Long-Life Microchannel Plate as a function of extracted output charge. After an initial burn-in period, in which the detector gain changes as a result of degassing, residual gas molecules from the inside of the channel, detector performance is very stable over a large amount of extracted output charge.

4. Resolving Rate and Lifetime issues of the MCP-PMT

We have developed a multi-pronged approach to addressing these problems focused on better quantifying the magnitude of the rate and lifetime issues, reducing the requirements on the PMT's by lowering the gain and optimizing the detector design, and pursuing industrial developments that promise to lead to a new long life MCP-PMT.

4.1 UTA Laser Tests

The tests are performed at the Picosecond Test Facility (PTF) in the Chemistry and Physics Research building at the University of Texas, Arlington. The PTF was established using funds from the Texas Advanced Research Program and the Department of Energy Advanced Detector Research program. The main components are a light-tight box containing a Hamamatsu PLP-10 pulsed picoseconds laser,

with 405 and 635 nm laser diode heads, various associated optical equipment (lenses, mirrors, beam splitters, and filters) , electronics (high voltage, discriminators, etc.), and a LeCroy 6 GHz Wavemaster 8620A oscilloscope. Figure 7 (a) shows the PTF and three undergraduate students who are currently supported by the Department of Energy to perform MCP-PMT tests . Figure 7 (b) shows a simple layout of the laser and optical elements, while Fig. 7 (c) shows the split signal incident on two channels of the Photonis 85011 64 channel MCP-PMT. The tests below were performed using the PLP-10 laser with the 405 nm laser diode head. The laser frequency can be varied over a range from 1 Hz to 100 MHz. Neutral density filters are used to control the amount of light, and a 4-channel MCP-PMT operating in the high light limit with a resolution of 6 ps, was used as a reference tube for timing studies.

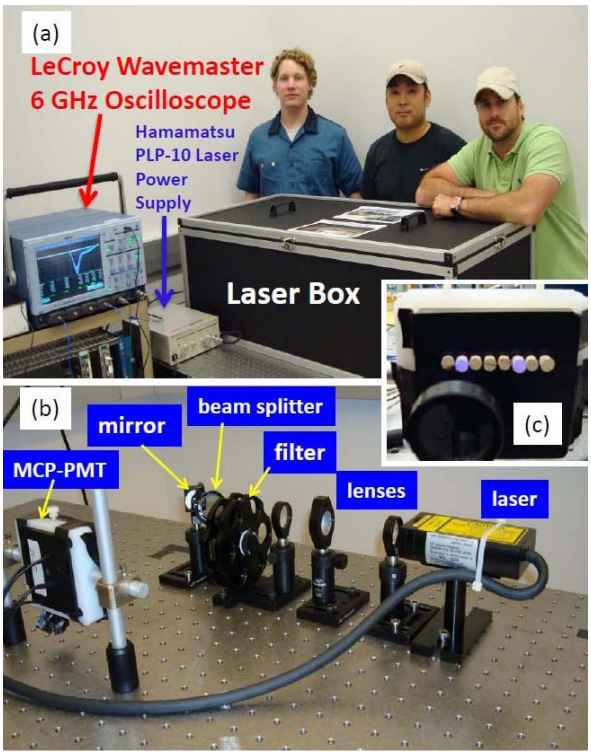

Figure 6: (a) UTA Picosecond Test Facility with the three undergraduate students who have been performing tests (b) an example layout of the laser and optical elements (c) the laser beams incident on the face of the 64 channel MCP-PMT.

Figure 7 shows a key result from the laser tests, namely that the timing for the 64 channel 10 μm pore Burle tube has very little dependence on gain down to gains significantly lower than the canonical 10^6! We note that there is very little dependence of the timing as a function of gain, with a measured time resolution of about 32 ps, for gains down to about 5 x10^4. This result is obtained using a beam size of about 0.2 cm^2 (a 5mm diameter beam centered in a 6 mm x 6 mm pixel) for a laser setting with 10 pe's, the working point of the QUARTIC detector, and is achieved with the appropriate combination of neutral

density filters, and approximated using the square of the ratio of the integrated area of the pulse divided by its width. We observe similar lack of timing dependence for various fixed numbers of photoelectrons. Thus this low gain operation does not result in a significant loss in timing resolution, but is equivalent to developing a tube with a 20 times higher current capability and 20 time longer lifetime than the standard tube (or equivalently, this reduces the magnitude of the discrepancy factor by a factor of 20).

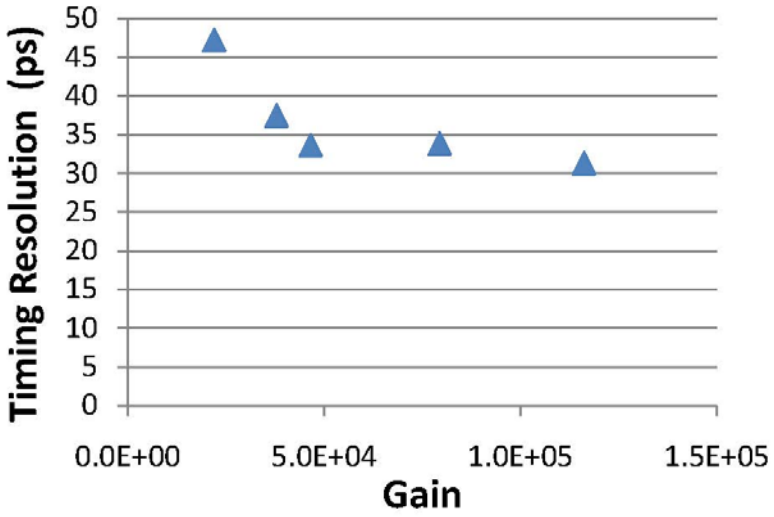

Figure 7: Timing resolution versus gain for the 64 channel 10 μm Burle Planacon tube.

We also measure the relative gain as a function of calculated output current. This is measured at our working point of 2350 V (a gain of about 5 x10^4) for 10 pe's. The measurement is made by determining the amplitude of the output pulse for various laser frequencies, and taking its ratio with respect to the average pulse height for a fixed frequency. The calculated output current is determined using Eq. 1, with R=laser frequency, N_{pe}=10, G= 5 x10^4 , and then scaling by the beam area of 0.2 cm^2. The results are shown in Fig. 8. We note for a laser frequency of 1 MHz, corresponding to a calculated current of about 0.4 μA/ cm^2 the relative gain is 78% (the extracted current of course is only 78% of this, about 0.3 μA/ cm^2), and the timing resolution is the same as for lower frequencies, so in fact, with this tube, we are able to operate comfortably at a rate within a factor of 10 of our expected maximum rate (1 MHz in an 0.2 cm^2 area compared to 15 MHz in a 0.36 cm^2), and uncomfortably (the last point was taken with a 10 MHz frequency) at the maximum expected rate. It seems clear that the high current version of the Photonis tube will not present any problem with our expected maximum rates.

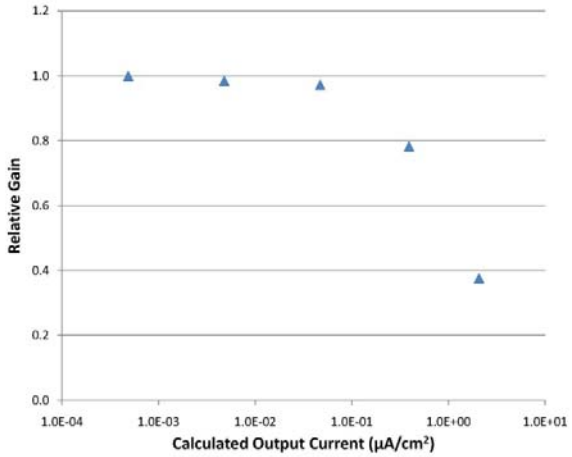

Figure 8: The relative gain for the 64 channel 10 μm Burle Planacon tube as a function of calculated output current.

4.2 Lifetime Tests

We note that lifetime studies are time consuming and expensive and notoriously unreliable as they often involve significant extrapolations. We thus plan to quantify the lifetime of current tubes using the UTA laser test stand to perform aging studies under conditions similar to our planned usage, to form a baseline in order to fully understand the magnitude of the problem. There is strong evidence for a wavelength dependence of aging results (shown earlier), where shorter wavelengths cause significantly less damage than longer ones (Cherenkov radiation is peaked in the UV). We have a 405 nm and 638 nm laser ideal for these tests.

4.3 Collaborating on Lifetime Issues

Nagoya have made substantial progress in understanding lifetime issues based on collaborations with Hamamatsu, and BINP also has had access to PMT construction. Following this model, we had many useful interactions with Burle, and they have provided us with several prototype tubes for tests, but due to internal reorganizations over the past couple of years, lifetime developments have been stalled. Now that internal issues have been resolved, they are again producing Planacons. We plan to obtain and test new versions of the tubes from Photonis that are being made using a new electron scrubbing technique that is expected to provide a factor of 5 to 10 improvement in the lifetime (based on tests by Photonis) by reducing positive ion contamination. We note that the first version of these better scrubbed tubes are expected to be available very soon (while Photonis have decided to stop producing standard PMT's they plan to vigorously continue efforts on MCP's due to large markets in image intensifiers and medical imaging).

Recently we began a collaboration with Arradiance, Inc. [12], a company that has demonstrated improved lifetime of MCP's, suppressing the traditional gain loss in the burn-in phase through deposition of thin films on the MCP's (Fig. 9). UTA has submitted a small business (SBIR Phase I) proposal with Arradiance aimed at improving the lifetime of the photocathode, by the aforementioned thin film application, which in addition to improving the lifetime and gain characteristics of the MCP, is expected to suppress ion production. The coating has also has been observed to give a factor of a few increase in gain, allowing the tube to be run at a lower voltage, reducing positive ion feedback. The proposal involves a program of R&D at Arradiance to optimize the thin film, and then apply the optimized film to MCP's obtained from Bruce Laprade (Vice President and General Manager of Photonis USA, Inc., Sturbridge, MA, the world's leading producer of advanced MCP's). Bruce will perform further tests, and certify that the Arradiance-modified MCP is safe to be installed in a Photonis Planacon MCP-PMT. Paul Hink, the Business and Development Manager of the Innovation & Technology Group, will oversee the installation of the MCP in the Photonis tube at the Lancaster, PA plant. Paul will then ship the tube to UTA for characterization. This SBIR feasibility study, if successful, will be followed by a Phase II proposal leading to the production of the improved long life tubes by mid-2012. This proposal was made possible through many discussions over the last nine months between myself and the principals, and the assistance of Emile Schyns, who is the Group Product Manager of the Photonis Microchannel Plate Division.

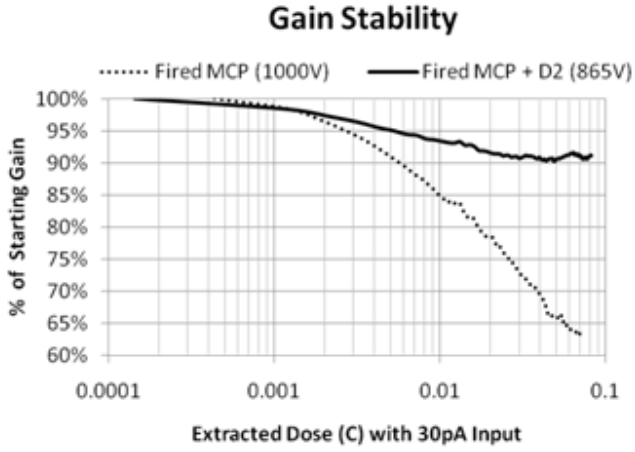

Figure 9: Arradiance D2 Film gain degradation vs. commercial MCP.

We have also developed a relationship with a smaller MCP-PMT producer, Photek, LTD. The University of Manchester, UC-London, and Bristol in consultation with UTA have submitted a developmental proposal for long life MCP-PMT's similar to the UTA-Arradiance SBIR. It involves inserting Arradiance coated MCP's into Photek MCP-PMT's, ion barrier MCP's, and MCP's with both

ion barriers and Arradiance coatings. In some ways the collaboration with Photek is even more promising than Photonis, as Photek is a small flexible company, and has shown great interest in custom MCP-PMT's, including developing a 16 or 32 channel configurable anode version of their 40 mm tube, which has the additional advantage that it could be constructed with 6 μm pores. Based on meetings this week (June 16, 2009), they have decided to make a four channel version of their 25 mm tube for initial tests, and we may have one as early as this fall to test at UTA. They are also open to the idea of a Z-stack (three MCP) version of a Photek MCP-PMT, and indeed have done this before for a space physics application.

Finally, we also note that Hamamatsu has recently produced a modified version of the SL-10, a one inch square 4-anode MCP-PMT with an ion barrier [13], in collaboration with the Nagoya group. We are investigating the possibility of a sixteen anode version of this tube, which would meet our needs, if it could be combined with better scrubbing or an Arradiance coating.

4.4 Optimizing Detector Design and Running Scenarios

The initial QUARTIC and GASTOF detectors were designed by FP420 for installation in the 420 m region. The addition of the 220 m group to the AFP proposal has stressed the timing detector performance requirements, as the 220 m single diffractive acceptance is approximately three times higher than the 420 m acceptance, resulting in a more demanding rate requirement of 15 MHz instead of 5 MHz proton rates, and significantly more multiple proton events. In addition to developing solutions to deal with the high 220 m rates and corresponding lifetime concerns, we have also been considering detector modifications to reduce the demands on MCP-PMT development. One very promising avenue that we are pursuing is the use of quartz fibers instead of quartz bars for the radiator of the QUARTIC detector. This would allow us to use finer bins in the *x* direction (perpendicular to the beam). Finer binning has the obvious benefit of improving the multiple proton timing (currently the protons must be in separate rows of the QUARTIC detector otherwise only the earlier one is timed, a situation that is mitigated by the planned offset by ½ a 6 mm bin of the second QUARTIC detector, but could still be improved upon by finer binning). Finer binning has the added benefit, that through appropriate routing of the fibers it would also allow the fibers to be mapped to pixels of the MCP-PMT in such a way as to equalize the proton rate in each pixel. We estimate that this will yield a factor of three reduction in the 220 m detector rates to the previously envisaged 5 MHz proton rates. This would also reduce the lifetime requirements to about 12 C/cm^2. We plan beam tests of quartz fibers this year.

We have not yet discussed the AFP version of the GASTOF detector. The baseline version of the GASTOF detector is not optimal for 220 m due to the lack of *x* segmentation. Krzysztof Piotrzkowski has mentioned a multi-anode version of GASTOF to deal with this issue. My preferred version involves converting GASTOF into GASTIC, namely using a multi-anode MCP-PMT (such as the Planacon or perhaps a Photek 32 channel 40 mm tube with 6 μm pores) in place of the current single channel one. Each of the 10 photoelectrons would typically go to a separate pixel, so the tube would be used in single pe mode at a gain of about 5 x 10^5. The single photon measurement would be on the order of 30 ps, but borrowing from the QUARTIC philosophy, there would be multiple measurements. A second proton in the same detector would mostly hit empty pixels, and by fitting the time distribution of all the hit pixels both protons could be timed, with comparable resolution to a single proton. Even rare three proton events would be distinguishable in this detector. A further advantage is that since no single measurement needs to be too precise, the same readout electronics could be used for GASTIC and QUARTIC. The average occupancy of a given pixel assuming a 30 MHz maximum rate at 220 m, would be 1 MHz in a 0.4 cm^2 area, at a gain of 5 x 10^5, so the current requirements would be a pedestrian 0.2 $\mu A/cm^2$, accessible with existing tubes. The lifetime requirements would correspondingly also be a modest 2 C/cm^2, achievable with any one of the proposed PMT modifications. We have begun simulations of the performance of a GASTIC detector and are in discussions about producing a suitably modified prototype for beam tests.

5. Outlook and Conclusions

Rate and lifetime concerns are serious issue for the MCP-PMT's to be used in the AFP timing detectors. The UTA laser tests showing that we can operate with a factor of 20 reduction in gain is a major step towards demonstration of a viable MCP-PMT solution, but in itself is not sufficient. Rate/current studies indicate that we are within about a factor of 10 of a solution, and, in fact, Photonis tubes with a factor of 10 better current performance have already been produced, so, although we have yet to obtain and test these tubes, we are confident that a solution to the rate issue is in hand, and will be demonstrated within the next year.

The lifetime issue has a larger discrepancy factor of perhaps 50, as current QUARTIC detector designs require a 35 C/cm^2 MCP-PMT. Many potential advances are envisaged to attain these long life MCP-PMT's. These include:

- Ion barrier, already demonstrated, this promises a factor 5 to 6 lifetime improvement (at the cost of a 40% collection efficiency reduction)
- Electron scrubbing, already demonstrated, this promises a factor 5 to 10 lifetime improvement
- Z-stack, already demonstrated, this promises a factor of 10 lifetime improvement

- Arradiance coated MCP's, to be demonstrated, this promises a factor of 10 or more lifetime improvement.

Various combinations of these factors are possible and should give multiplicative improvement factors, except for the electron scrubbing and Arradiance coating, which would be expected to be orthogonal. In parallel with the development of a long life tube, we are pursuing new detector designs (quartz fiber radiator, multi-anode GASTOF) that have the potential to dramatically reduce the rate and lifetime requirements. Finally, we also note that recent physics studies indicate that the 220 m acceptance for the expected closest location of the detectors with respect to the beam reduces the predicted acceptance of background diffractive protons by a factor of nearly two, and that the integrated charge assumed in a year was based on continuous operation at 10^{34} $cm^{-2}s\text{-}^{1}$, more realistic running scenarios result in an average instantaneous luminosity of perhaps one-half this, reducing the burden on the tubes by another factor of two. In summary, given approval to proceed to TDR, we can better pursue the funding necessary to develop a fast timing system to operate at 10^{34} $cm^{-2}s\text{-}^{1}$, and we have no doubt that this can be achieved with MCP-PMT technology.

References

[1] http://www.photonis.com.

[2] Paul Hink, private communication.

[3] Super B Conceptual Design Report, Presented to INFN, March 2007, http://www.pi.infn.it/SuperB/?q=CDR; Thomas Hadig, hep-ex/0304028.

[4] http://superb.kek.jp/

[5] The PANDA Collaboration, "Physics Performance Report for PANDA: Strong Interaction Studies with Antiprotons," arXiv:0903.3905v1 [hep-ex] (2009); K.Fohl et al., "The DIRC detector of the PANDA experiment at FAIR," Nucl. Instr. and Meth. **A595**, p.88, (2008).

[6] http://cp3.phys.ucl.ac.be/upload/talk/CP3-09-06.pdf

[7] http://www.nightvision.com/products/military/case_study-gen3.htm

[8] M. Akatsu, et al., Nucl. Instr. and Meth. A 440 (2000) 124; M. Akatsu, et al., Nucl. Instr. and Meth. A 528 (2004) 763;Y. Enari, et al., Nucl. Instr. and Meth. A 547 (2005) 490.

[9] N. Kishimoto, et al., Nucl. Instr. and Meth. A 564 (2006) 204.

[10] A.Yu. Barnyakov, et al., Nucl. Instr. and Meth. A 598 (2009) 160.

[11] http://www.kore.co.uk/mcp-faq.htm.

[12] http://www.arradiance.com

[13] K. Inami, "Development of a TOP Counter for Super B Factory," Workshop on Fast Cerenkov Detectors, Giessen, Germany, https://indico.gsi.de/conferenceDisplay.py?confId=529.

AFP Silicon Tracker

Glasgow, Manchester, Saclay

Update 4 July 2009

1. Introduction

This document updates progress on the silicon trackers at 220 and 420 for the AFP detector system. Progress is in two areas – improving the radiation tolerance and conceptual design for the 220 m silicon tracker. These are detailed below.

2. Radiation tolerance of the front-end readout chip

The 3D sensor is radiation hard to 1-2 10^{16} charged particles per cm^2. However, the FE-I3 ATLAS pixel readout chip which uses 0.25 micron technology is radiation hard to ~$2x10^{15}$ charged particles per cm^2 or ~50 Mrad. This is the nominal specification although operation upto 100 Mrad has been reported [1].

Calculations by FP420 – fig 44 ref [2] - are compatible with those made by TOTEM – fig 5.1 ref. [3]. There is an intense but highly localised dose in the inner four square mm of the detector close to the beam. This falls rapidly both horizontally and vertically. The dose is entirely due to protons coming from diffractive events at the interaction point. The flux is around $4x10^7$ protons $cm^{-2}s^{-1}$ at a luminosity of 10^{34} $cm^{-2}s^{-1}$. In a year this corresponds to $4x10^{15}$ protons cm^{-2} or 100 Mrad. Thus the FE-I3 would fail after one year in this region taking 100 Mrad as the maximum permissible dose.

There are two possible solutions.

i) The dose is highest in very narrow vertical band. By moving the sensors up and down by 0.5 to 2 mm the dose can be evened out. This technique was used with charge coupled devices in NA32. This technique would give a factor three improvement in the lifetime, or around 3 years at L= 10^{34} $cm^{-2}s^{-1}$. This is an additional specification for mechanical design. It has been discussed with the engineers and can be implemented. This is explained in more detail below.

The profile of hits in y (vertical) at 220 m and 420 m are shown in Figs. 1 to 2. A Guassian fit to these is shown. It is easy to show that by adding three Gaussian's for y = nominal, y = nominal + 2.4σ and y = nominal - 2.4σ one obtains roughly a flat distribution in which the overall intensity is 1/3 relative to adding them all together at the nominal y value. In other words, the intensity is reduced by a factor 1/3. Table 1 shows the σ for the various cases. It also indicates how much of the sensor/readout chip Y acceptance is required to keep all the hits contained including a shift of 2.4σ either side of the initial position. The acceptance is covered by 1 or 2 FE-I3 readout chips for 420 m and 220 m respectively. There is just enough room to move the sensors to three positions in Y with the FE-I3 readout chip, thus reducing the dose by a factor three.

Table 1 Distribution of diffractive hits at 220 and 420 m and required shift and acceptance

Condition	Required Y acceptance close to beam (mm)	σ (mm)	Shift 2.4σ (mm)	Acceptance + 2xshift (mm)	FE-I3 Y range (mm)	FE-I4 Y range (mm)
220 Side 1	12	0.45	1.1	14.2	16	20
220 Side 2	12	0.7	1.7	15.4	16	20
420 Side 1	5.5	0.22	0.53	7.1	8	20
420 Side 2	5.5	0.5	1.2	7.9	8	20

ii) The FE-I4 chip is being developed for the IBL project. This is approximately double the size vertically and horizontally. This uses 0.13 micron technology and is known to be a factor 4 more radiation tolerant than the FE-I3 or 200 Mrad, [4]. This would give a two year lifetime for the inner FE-I4 readout chips. Moreover, as Table 1 shows, a factor three in addition can be achieved by moving the tracker in Y and because the FE-I4 sensor is larger than the FE-I3, this could be repeated at least a further two times. Thus the FE-I4 would give ten years at $L = 10^{34}$ $cm^{-2}s^{-1}$.

3. Silicon layout at 220 m

For reference, figure 3 shows the 420 m design on which the 220 m tracker is based. It uses three FE-I3 chips per superlayer. Figure 4 shows the 220 m design which uses six FE-I3 chips per superlayer. Figure 5 gives plan views of the design.

4. FE-I4 versus the FE-I3

Table 2 summarises the parameters of the FE-I3 and FE-I4 readout chips. The FE-I3 is used in the current ATLAS pixel detector. The FE-I4 is under development for the Insertable B-Layer (IBL) project and operation at the proposed SLHC. As noted above, the FE-I4 would give an improvement in the overall radiation tolerance due to the fact that the technology is a factor four harder, and more vertical shifts are possible to even out the dose.

Table 2 Comparison of the FE-I3 and FE-I4 front-end readout chips

Chip	**Pixel Size (μm^2)**	**Number in x and y**	**Dimension (mm)**	**Maximum Dose (Mrad)**
FE-I3	50 x 400	144 x 20	7.2 x 8.0	50-100
FE-I4	50 x 250	336 x 80	16.8 x 20	200

The first FE-I4 chips will not be available until late 2010 with IBL modules expected at the end of that year. This chip is better matched for the 220 events and would simplify the superlayer design. A common superlayer design for 220 and 420 also has advantages. We have close contact with the R&D for the IBL project and may use this readout chip if progress is good in 2010. 3D sensors matched to the FE-I4 chip are on the latest SINTEF 3D silicon sensor mask which will finish processing later this year.

References

[1] M. Garcia-Sciveres, Dortmund Planar Sensor Workshop, June 2007.
[2] "The FP420 R&D Project: Higgs and New Physics with forward protons at the LHC", http://arxiv.org/abs/0806.0302.
[3] TOTEM TDR, TOTEM Collaboration, LHCC-2004-002, 2004.
[4] "A new ATLAS pixel front-end IC for upgraded LHC luminosity", M. Barbero et al., Nucl. Instr. Meths. A 604 (2009) 397–399.

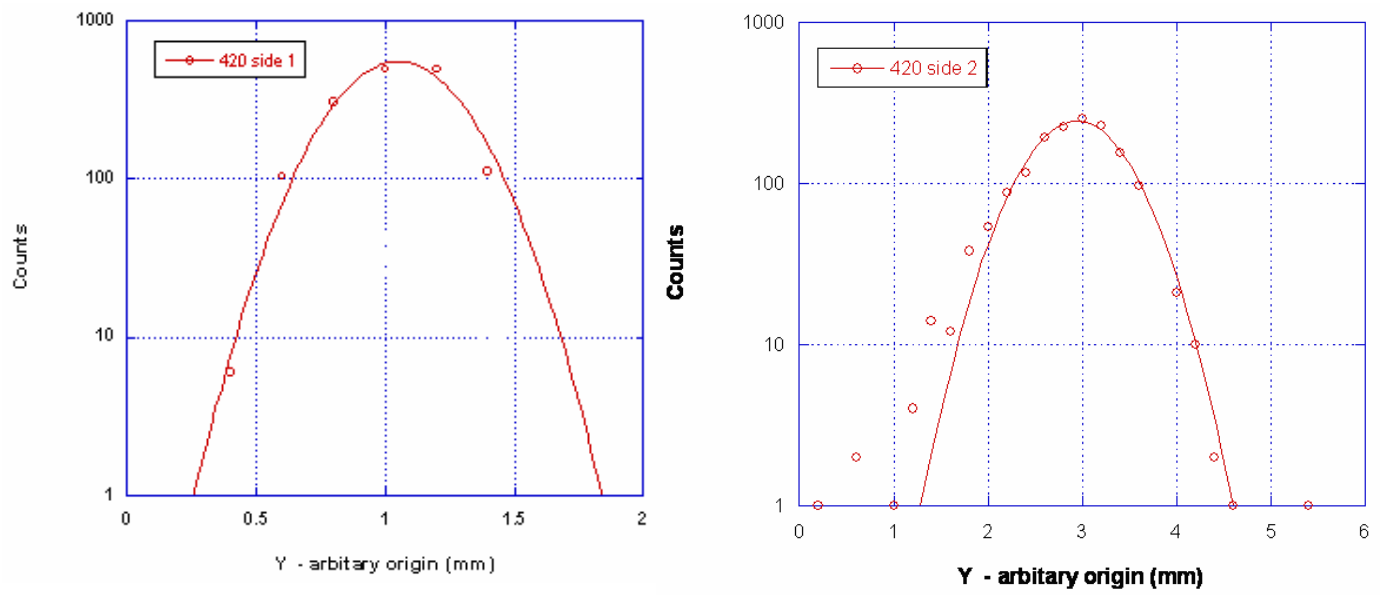

Figure 1. Diffractive hits in vertical direction at 420 m. The curves show a Gaussian fit with a sigma of 0.22 and 0.5 mm for sides 1 and 2 respectively.

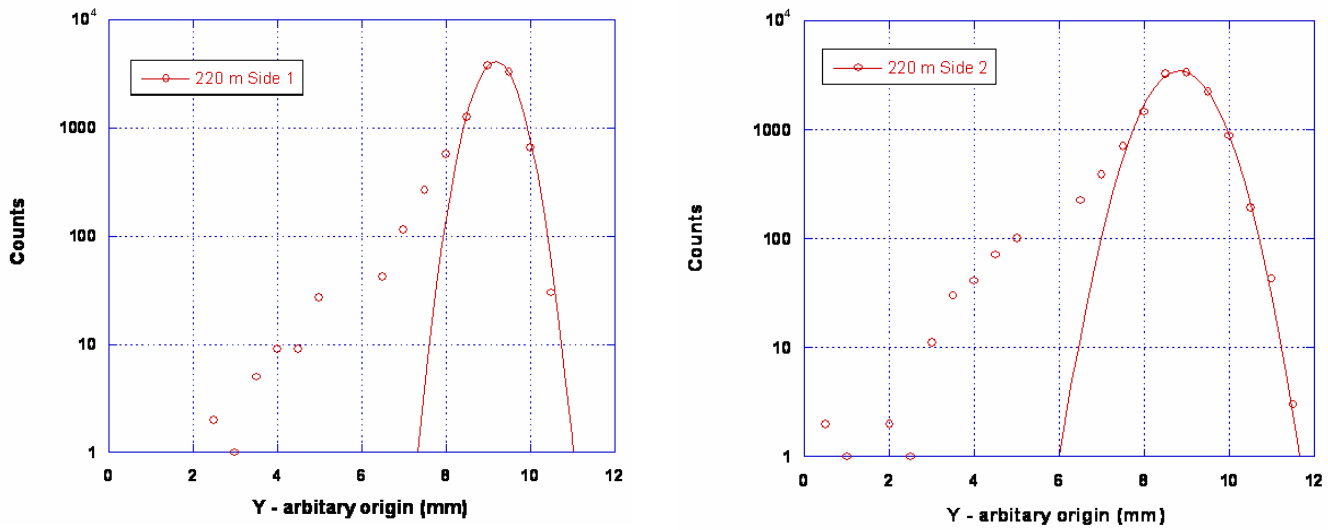

Figure 2. Diffractive hits in vertical direction at 420 m. The curves show a Gaussian fit with a sigma of 0.45 and 0.7 mm for sides 1 and 2 respectively

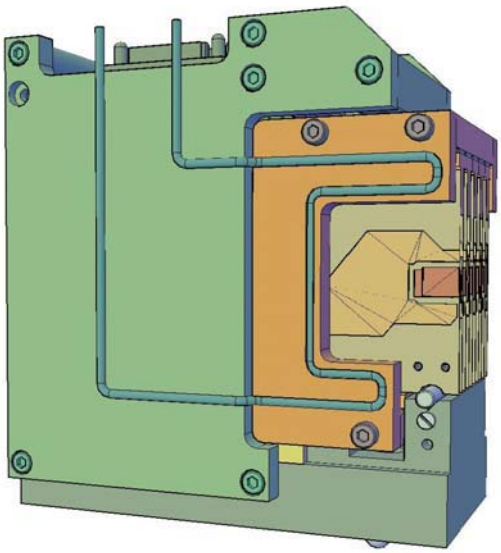

Figure 3. 420 m silicon tracker design. Three 3D/FE-I3 detectors are used horizontally in each superlayer to cover the acceptance. Only one can be seen in this view.

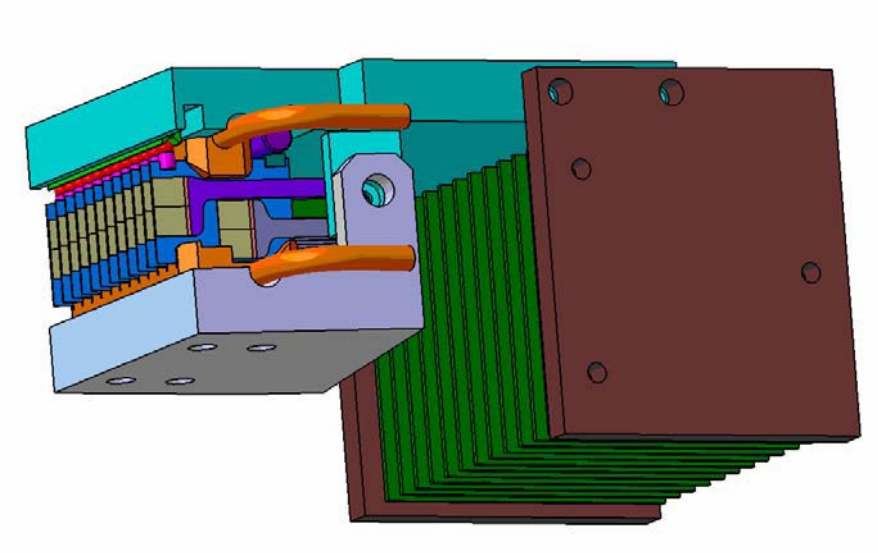

Figure 4 220 m silicon tracker design. Six 3D/FE-I3 detectors are used horizontally in each superlayer to cover the acceptance. Only four can be seen in this view.

Figure 5 - 220 m Silicon Tracker Conceptual Design